Journal of Natural Fibers

ISSN: 1544-0478 (Print) 1544-046X (Online) Journal homepage: www.tandfonline.com/journals/wjnf20

Unraveling the Pyrolysis Mechanisms of *Syagrus* Palm Waste Fibers Through Gaussian Deconvolution and Kinetic Modeling

Oussama Ferfari, Ahmed Belaadi, Hassan Alshahrani, Djamel Ghernaout & Herbert Mukalazi

To cite this article: Oussama Ferfari, Ahmed Belaadi, Hassan Alshahrani, Djamel Ghernaout & Herbert Mukalazi (2025) Unraveling the Pyrolysis Mechanisms of *Syagrus* Palm Waste Fibers Through Gaussian Deconvolution and Kinetic Modeling, Journal of Natural Fibers, 22:1, 2562473, DOI: 10.1080/15440478.2025.2562473

To link to this article: https://doi.org/10.1080/15440478.2025.2562473

JOURNAL OF NATURAL FIBERS
2025, VOL. 22, NO. 1, 2562473
https://doi.org/10.1080/15440478.2025.2562473

Unraveling the Pyrolysis Mechanisms of *Syagrus* Palm Waste Fibers Through Gaussian Deconvolution and Kinetic Modeling

Oussama Ferfari[a], Ahmed Belaadi[a], Hassan Alshahrani[b], Djamel Ghernaout[c,d], and Herbert Mukalazi[e]

[a]Department of Mechanical Engineering, Faculty of Technology, Skikda, Algeria; [b]Department of Mechanical Engineering, College of Engineering, Najran University, Najran, Saudi Arabia; [c]Chemical Engineering Department, College of Engineering, University of Ha'il, Ha'il, Saudi Arabia; [d]Chemical Engineering Department, Faculty of Engineering, University of Blida, Blida, Algeria; [e]Department of Mathematics and Statistics, Kyambogo University, Kampala, Uganda

ABSTRACT

The thermal decomposition kinetics and thermodynamics of *Syagrus romanzoffiana* waste rachis fibers (*Sr*WRFs) were investigated through thermogravimetric analysis in a nitrogen atmosphere at heating rates (β) of 30, 40, and 50°C/min. The Coats–Redfern method was employed to determine kinetic parameters, including activation energy (E_a), pre-exponential factor (A), and reaction mechanisms. In contrast, thermodynamic properties such as enthalpy change (ΔH), Gibbs free energy (ΔG), and entropy change (ΔS) have been derived to evaluate the energy requirements and spontaneity of the pyrolysis process. A three-parallel Gaussian reaction model was employed to deconvolute the degradation profiles of hemicellulose, cellulose, and lignin, revealing distinct temperature intervals for each component: hemicellulose (200–345°C), cellulose (305–398°C), and lignin (220–650°C), with high fitting accuracy ($R^2 \geq 0.99537$). The kinetic analysis identified sigmoidal rate (SR) models (SR6, SR7, and SR8) as the most suitable, yielding E_a values ranging from 97.31 to 262.11 kJ/mol, which increased with higher heating rates. Thermodynamic results indicate that *Sr*WRF pyrolysis is endothermic ($\Delta H > 0$) and non-spontaneous ($\Delta G > 0$), with negative entropy changes (ΔS) suggesting an increase in molecular order among the degradation products. The kinetic compensation effect was confirmed, demonstrating a linear relationship between ln$A$ and E_a.

摘要

通过在氮气气氛中以30、40和50°C/min的加热速率 (β)进行热重分析，研究了罗马冷杉废纤维 (SrWRFs)的热分解动力学和热力学. 采用Coats-Redfern方法确定动力学参数，包括活化能 (Ea)、指数前因子 (A)和反应机理. 相比之下，已经推导出了焓变(ΔH)、吉布斯自由能 (ΔG)和熵变 (ΔS)等热力学性质，以评估热解过程的能量需求和自发性. 采用三平行高斯反应模型来解卷积半纤维素、纤维素和木质素的降解曲线，揭示了每种成分的不同温度区间: 半纤维素 (200-345°C)、纤维素 (305-398°C)和木质素 (220-650°C)，拟合精度很高 (R^2 ≥0.99537). 动力学分析确定S形速率 (SR)模型 (SR6、SR7、SR8)是最合适的，Ea值范围为97.31至262.11 kJ/mol，随着加热速率的增加而增加. 热力学结果表明，SrWRF热解是吸热的 ($\Delta H > 0$)和非自发的 ($\Delta G > 0$)，负熵变 (ΔS)表明降解产物之间的分子顺序增加. 动力学补偿效应得到证实，表明lnA和E之间存在线性关系.

KEYWORDS

Syagrus romanzoffiana waste rachis fibers (*Sr*WRFs); pyrolysis kinetics; Coats–Redfern method; thermodynamic analysis; Gaussian deconvolution

关键词

罗曼索菲亚冷杉 (Syagrus romanzoffiana)废轴纤维 (SrWRFs); 热解动力学; Coats-Redfern法; 热力学分析; 高斯反卷积

Introduction

The increasing global energy demands and the ongoing depletion of conventional fuel sources underline the urgent necessity for sustainable and environmentally friendly energy alternatives (Bongomin, Nziu, and Akgül 2022). The consumption of fossil fuels must be systematically regulated due to their limited availability and substantial environmental impacts, including global warming and air pollution. In this context, lignocellulosic biomass waste, a renewable byproduct of agriculture, forestry, and production activities, has gained prominence as a viable energy source (Ferfari et al. 2024; Reddy et al. 2023).

CONTACT Ahmed Belaadi ahmedbelaadi1@yahoo.fr; a.belaadi@univ-skikda.dz Department of Mechanical Engineering, Faculty of Technology, University 20 August 1955- Skikda, El-Hadaiek, Skikda, Algeria; Herbert Mukalazi hmukalazi@kyu.ac.ug Department of Mathematics and Statistics, Kyambogo University, Kampala, Uganda

Supplemental data for this article can be accessed online at https://doi.org/10.1080/15440478.2025.2562473.

Conventional waste treatment methods, including disposal techniques such as landfills and incineration, have substantial ecological disadvantages. Landfills occupy a considerable amount of land and pose a risk of contaminating soil and water resources due to leaching from waste deposits (Abdel-Shafy and Mansour 2018; Abubakar et al. 2022). Meanwhile, incineration releases hazardous pollutants, including greenhouse gases, which worsen air quality and raise public health concerns (Ferronato and Torretta 2019). While biomass waste can serve as an energy source, its high oxygen and moisture content result in a low energy density (Vyazovkin and Muravyev 2024). To address this limitation, thermochemical conversion processes, such as pyrolysis and combustion, are utilized to transform raw biomass into higher-quality fuels and valuable chemical intermediates (Ashraf et al. 2023; Azam et al. 2024). The increasing industrial and scientific interest in biomass-derived energy has heightened the need to comprehend its micro-scale thermochemical behavior (Zhong et al. 2023; Zhu et al. 2021). Predicting thermal degradation kinetics across a broad range of heating rates (β) remains a challenge, especially in microgravimetric analysis (Ding et al. 2023). Addressing these gaps is crucial for optimizing biomass conversion technologies and advancing renewable energy solutions.

The thermal decomposition of biomass has been studied using both model-free and model-fitting kinetic approaches (Fischer, Lemaire, and Bensakhria 2024; Najafi, Rezaei Laye, and Sobati 2024; Steven et al. 2024). Thermal decomposition kinetics is often evaluated using model-free techniques, notably the Flynn–Wall–Ozawa, Friedman, Starlink, and Kissinger–Akahira–Sunose methods (Arumugam and Ganesan 2024; Y. Wang et al. 2024a). Alternatively, model-fitting approaches such as the direct Arrhenius method (Kumar Shrivastava and Prasad Chakraborty 2024), the Coats–Redfern method (CRM) (Hadou et al. 2024a), the Kennedy–Clark method (B. Li et al. 2024), the Criado master plot (CMP) (Choudhary et al. 2024; B. Y. Li et al. 2023), and the Distributed Activation Energy Model are also widely used (Choudhary et al. 2024; B. Y. Li et al. 2023). Model-free methods enable kinetic analysis without assuming a specific reaction mechanism; however, they typically require large datasets (Hadou et al. 2025). In contrast, model-fitting techniques such as the CRM offer a more straightforward approach by assuming a first-order reaction and using a linearized Arrhenius equation to estimate the activation energy (E_a) and the pre-exponential factor (A) from thermogravimetric analysis (TGA) data. This characteristic makes them valuable for initial kinetic studies (Choudhary et al. 2024; B. Y. Li et al. 2023).

The industrialization of biomass pyrolysis requires a comprehensive kinetic and thermodynamic analysis. Kinetic parameters – E_a, A, and reaction order – enable optimized reactor design (Ascher, Watson, and You 2022; Clemente-Castro et al. 2023Nasfi, Carrier, and Salvador 2022), process control (Gupta et al. 2024; Lei et al. 2023), and improved energy efficiency (Liu et al. 2024; Osman, Nasr, et al. 2024; Zhang et al. 2024). Thermodynamic properties – enthalpy (ΔH), entropy (ΔS), and Gibbs free energy (ΔG) – predict product yields (Amoloye, Abdulkareem, and Adeniyi 2023), guide heat recovery (Amoloye, Abdulkareem, and Adeniyi 2023), and assess feedstocks (Osman, Fang, et al. 2024; Vanisree, Chandran, and Aparna 2024). Integrating these approaches enhances pyrolysis technology, improves process efficiency, and facilitates sustainable scale-up (Osman, Fang, et al. 2024; Vanisree, Chandran, and Aparna 2024). This integrated framework enhances reactor optimization and the commercial viability of biomass conversion systems.

Integrating kinetic and thermodynamic analysis optimizes biomass pyrolysis by enhancing predictive reactor modeling (Lingamdinne et al. 2024), facilitating techno-economic evaluations that balance reaction rates and energy demands (Dai et al. 2024), and developing efficient conversion systems that maximize yields while minimizing energy consumption (Lalaymia et al. 2025). This approach accelerates the commercialization of waste-to-value technologies, promotes circular economies, and reduces reliance on fossil fuels (Nath 2024, Samuel Olugbenga et al. 2024). Continued refinement of these methodologies remains essential for developing sustainable biorefineries and achieving global decarbonization targets (V. K. Kumar, Hallad, and Panwar 2024; Rashd et al. 2024), underscoring the importance of fundamental research in driving practical solutions for renewable energy and waste valorization.

Studies have thoroughly examined the thermal decomposition behavior and kinetic parameters of different types of biomass in both oxygen-rich and inert environments (Elmay et al. 2016). Among the kinetic parameters, E_a is acknowledged as the most critical factor influencing biomass reactivity (Mian et al. 2019a). Research on date palm residues has revealed considerable variability in kinetic parameters, stemming from differences in experimental methodologies, operating conditions, and β values. This variability complicates comparisons across various studies (El May et al. 2012).

Chen et al. (Chen, Li, Xu, et al. 2019) investigated the pyrolysis of micron-scale poly(methyl methacrylate) (PMMA) waste using thermogravimetry (TG) at various β values (5–40°C/min). By using isoconversional and model-fitting methods (i.e., CRM), they found that the degradation follows the kinetic model $g(\alpha) = (1 - \alpha)^{-1/2} - 1$. E_a (243.69 kJ/mol) and A (1.19×10^{19} min^{-1}) were significantly higher than those of conventional PMMA, highlighting the influence of particle size. The model accurately predicted pyrolysis behavior, offering valuable insights into the recycling of PMMA waste.

Raza and Abu-Jdayil (Raza and Abu-Jdayil 2023) investigated the co-pyrolysis of date palm seeds and cashew nut shells at a β of 10°C/min using TG. A 50:50 mix showed a 9% lower E_a than pure cashew shells, indicating synergy. Decomposition occurred through diffusion mechanisms (DMs), resulting in stable biochar with enhanced energy efficiency. Although the process was endothermic and non-spontaneous, the researchers demonstrated the potential to convert agricultural waste into valuable products through pyrolysis, offering sustainable resource recovery solutions for arid regions.

Bongomin et al. (Bongomin et al. 2024) investigated the breakdown of five types of biomass waste using TGA and identified three stages: drying, devolatilization, and char formation. The macadamia nutshell exhibited the highest reactivity, showing the earliest devolatilization at 175°C and a peak at 380°C. In contrast, the coffee husk displayed the lowest E_a (60.59 kJ/mol) and the best spontaneity, with $\Delta G = 148.34$ kJ/mol. Reactivity indices ranked macadamia nutshell as the most reactive and rice husk as the least reactive.

Lalaymia et al. (Lalaymia et al. 2024) investigated the pyrolysis characteristics of *Agave americana* flower stalk (FS*Aa*) fibers using TGA at a β of 5–20°C/min with CRM. The multi-stage decomposition demonstrated high accuracy ($R^2 > 0.99$), with E_a values ranging from 83.6 to 210.1 kJ/mol. Negative entropy values indicated an ordered transition state during degradation.

The thermal decomposition behavior of *Syagrus romanzoffiana* waste rachis fibers (*Sr*WRFs) under various processing conditions has received limited attention in recent research, particularly in terms of determining kinetic parameters and decomposition pathways. This pioneering work addresses the knowledge gap through systematic TGA of *Sr*WRF samples subjected to previously unstudied high β rates of 30, 40, and 50°C/min. The novelty of our modeling approach lies in applying high-β thermogravimetry combined with a three-Gaussian deconvolution tailored to the unique decomposition characteristics of *SrWRFs*, which has not been extensively explored in prior literature. The Coats–Redfern method was selected for its reliability in modeling non-isothermal TGA data at high β values with minimal computational complexity. Gaussian deconvolution was employed due to its superior resolution in separating overlapped DTG peaks compared to isoconversional or distributed activation energy methods, which require broader conversion datasets. This dual approach ensures both mechanistic clarity and practical applicability. The innovative combination of isoconversional and mechanistic modeling approaches provides a novel understanding of the thermal degradation patterns and energy barriers involved in *Sr*WRF pyrolysis. These original findings enable the precise simulation of fiber behavior under thermal stress, thereby promoting their potential application in sustainable material engineering and renewable energy innovations. The study makes a significant contribution to both fundamental biomass science and the advancement of practical green technologies by characterizing this promising yet underexplored natural resource. The results provide essential design parameters for utilizing *Sr*WRFs in sustainable manufacturing processes and energy systems, supporting the shift toward circular bioeconomy models.

Materials and methods

Materials

The *Sr*WRFs in this study displayed diameters varying from 120 to 160 µm and a density of 1.23 g/cm^3, consistent with the earlier findings of the research group (Ferfari et al. 2023). Extracting *Sr*WRFs took place in Algeria, utilizing the traditional water retting method. Before analysis, the fibers underwent a thorough cleaning process using water to remove impurities, followed by natural air-drying to preserve their structural integrity. For experimental purposes, fiber segments ranging from 2 to 5 mm were selected. Figure 1 illustrates the isolation and processing methodology.

Figure 1. Process of extracting fibers from *Syagrus* palm rachis waste.

Physicochemical analysis for SrWRFs

To analyze the physicochemical properties of *Syagrus romanzoffiana* waste rachis fibers (*Sr*WRFs), a combination of proximate and ultimate analyses was conducted (Table 2). Proximate analysis, performed following standard GB/T 212–2008, involved a muffle furnace to determine fixed carbon, volatile matter, and ash content (Y. Wang et al. 2023a). Meanwhile, ultimate analysis using a CHNS/O elemental analyzer quantified carbon, hydrogen, nitrogen, and oxygen concentrations (I. Ali et al. 2021a). This dual-method approach enabled a thorough characterization of *Sr*WRFs, integrating elemental composition with thermal degradation behavior for a complete material profile.

Thermogravimetric analysis (TGA) of Syagrus romanzoffiana waste rachis fibers (SrWRFs)

To evaluate the thermal stability of *Sr*WRFs, TGA was performed using a METTLER TOLEDO TGA/DSC 3 + analyzer (1600°C, Constantine, Algeria). Fiber samples weighing 5–10 mg were heated from ambient temperature to 800°C at different rates ($\beta = 30$, 40, and 50°C/min) in a nitrogen atmosphere to prevent oxidative degradation. The weight loss (WL) profiles obtained from TGA offer insights into the thermal decomposition behavior of the fibers. Moreover, the data helped identify the kinetic and thermodynamic parameters, thereby enhancing the understanding of the degradation mechanisms. Strict experimental controls were maintained to ensure precision and minimize errors during the analysis. Each TGA experiment was conducted in triplicate under a constant nitrogen flow of 100 mL/min, using calibrated temperature profiles and a controlled sample mass ranging from 5 to 10 mg. Experimental reproducibility was confirmed by achieving less than 3% variation in weight loss and DTG peak temperatures across all runs (Raza et al. 2022a).

Three-parallel Gaussian reaction model approach

The thermal decomposition behavior of biomass was analyzed through deconvolution using a three-parallel Gaussian reaction model, which mathematically separates the complex degradation profile into three distinct pseudo-components (P-components) representing hemicellulose (P-HCL), cellulose (P-CL), and lignin (P-LG) (Equation (1)). This method enables the individual kinetic analysis of each biomass component by fitting Gaussian distributions to their corresponding decomposition temperature ranges within the

overall TG curve. The model offers enhanced accuracy in describing the multi-stage degradation process characteristic of lignocellulosic materials.

$$y = y_0 \frac{A b \exp\left(\frac{-4\,ln(2)(x-x_c)^2}{w^2}\right)}{w\sqrt{\frac{\pi}{4\,ln\,(2)}}} \tag{1}$$

In the Gaussian deconvolution model, the parameters y_0, x_c, and w represent the baseline offset, the peak center position (indicating the characteristic decomposition temperature), and the peak width (denoting the temperature range of decomposition), respectively. These variables together define the shape, position, and amplitude of each P-component's thermal degradation profile in the multi-peak fitting analysis.

Residuals were computed as the point-by-point difference between experimental DTG data and the fitted Gaussian model curves (Fischer, Lemaire, and Bensakhria 2024):

$$Residual(T) = \left(\frac{d\alpha}{dT}\right)_{exp} - \left(\frac{d\alpha}{dT}\right)_{fit} \tag{2}$$

Residual plots were generated for each heating rate (30, 40, and 50°C/min) to evaluate model accuracy and detect potential systematic errors. In addition, the root mean square error (RMSE) was calculated to provide a quantitative measure of goodness of fit, defined as:

$$RMSE = \sqrt{\frac{1}{n}\sum_{i=1}^{n}\left[\left(\frac{d\alpha}{dT}\right)_{i,exp} - \left(\frac{d\alpha}{dT}\right)_{i,fit}\right]^2} \tag{3}$$

where n is the number of data points. Low RMSE values, combined with randomly distributed residuals, indicate robust model performance beyond what can be inferred from correlation coefficients (R^2) alone (Lalaymia et al. 2024).

Kinetic analysis

The thermal decomposition kinetics of *Sr*WRFs have been analyzed using the CRM. This modeling approach not only identifies the reaction mechanism but also enables the calculation of key kinetic parameters, including E_a and A. The fundamental equation that governs the CRM can be expressed as follows (Gayathri et al. 2020):

$$\ln\left[\frac{g(\alpha)}{T^2(K)}\right] = \ln\left[\frac{AR}{\beta E_a}\right]\left(1 - \frac{2RT}{E_a}\right) - \frac{E_a}{RT} \tag{4}$$

This method offers valuable insights into the thermal degradation behavior of natural fibers by mathematically describing the relationship between temperature and reaction rate under non-isothermal conditions. The analysis was particularly useful for understanding the multi-stage degradation process that is characteristic of lignocellulosic materials, such as *Sr*WRFs.

The term $2RT/E_a$ was determined to be significantly less than one ($2RT/E_a << 1$), which permitted its simplification in the kinetic analysis (Sait et al. 2012). As a result, the thermal decomposition behavior was evaluated using Equation (5):

$$\ln\left[\frac{g(\alpha)}{T^2(K)}\right] = \ln\left[\frac{AR}{\beta E_a}\right] - \frac{E_a}{RT} \tag{5}$$

In the kinetic model, $g(\alpha)$ describes the reaction mechanism, where α (Equation (6)) measures the extent of conversion (Naqvi et al. 2015). The analysis employs β (°C/min), the gas constant R (8.314 J/mol·K), and A (min^{-1}) to determine the decomposition kinetics via the rate constant K.

$$\alpha = \frac{W_0 - W_t}{W_0 - W_f} \tag{6}$$

Equation (6) quantitatively illustrates the progression of the degradation procedure.

The thermal degradation of the *Sr*WRFs was kinetically analyzed using the Arrhenius method, which describes the exponential relationship between the reaction rate and temperature. Equation (7) expresses this fundamental principle (Raza et al. 2022a):

$$k(T) = A \times \exp\left(-\frac{E_a}{RT}\right) \tag{7}$$

The kinetic parameters (E_a and A) can be determined through linear regression analysis of $\ln[(g(\alpha))/(T^2]$ *vs.* $1/T$. The resulting plot yields a slope of $-E_a/R$, and its intercept is $\ln[AR/(\beta E_a)]$. Here, $g(\alpha)$ denotes the kinetic model function (dependent on the reaction mechanism), T represents the absolute temperature (K), β indicates the heating rate (°C/min), and R is the universal gas constant.

For biomass decomposition studies, appropriate g (α) functions were selected from Table 1 to model the solid-state degradation processes. This Arrhenius-type analysis enables simultaneous determination of both *E*a and *A* from a single TG experiment.

The thermal decomposition kinetics of *Sr*WRFs were investigated using CRM, combined with 36 solid-state reaction models categorized into four mechanistic groups: chemical process (CP), acceleratory rate (AR), sigmoidal rate (SR), and deceleratory rate equations. This non-isothermal approach facilitated the determination of key kinetic parameters, including E_a, A, and the correlation coefficient (R^2), with the optimal model chosen based on both the best fit to the kinetic function $g(\alpha)$ and the highest R^2 value.

The analysis focused on the principal decomposition stage (i.e., Stage II), with temperature ranges of 210–385°C (30°C/min), 232–415°C (40°C/min), and 251–436°C (50°C/min) corresponding to the significant WL regions observed at various β values.

Thermodynamic investigation

The thermodynamic properties of *Sr*WRFs, including Gibbs free energy (ΔG), enthalpy change (ΔH), and entropy change (ΔS), were derived from TG data using previously determined CRM kinetic parameters. These thermodynamic quantities were calculated using fundamental relationships that connect kinetic and thermodynamic analyses of thermal decomposition processes.

The evaluation employed Equations (8)-(10) to characterize the energy requirements and spontaneity of the degradation reactions (I. Ali et al. 2021b):

$$\Delta H = E_a - RT_m \tag{8}$$

$$\Delta G = E_a + RT_m ln\left(\frac{K_B T_m}{hA}\right) \tag{9}$$

$$\Delta S = \frac{\Delta H - \Delta G}{T_m} \tag{10}$$

Criado master plot (CMP) method

The CMP method employs a direct model-fitting technique to identify the kinetic reaction mechanism of pyrolysis, as outlined in Equation (11) (Choudhary et al. 2024):

$$\frac{Z(\alpha)}{Z(0.5)} = \frac{f(\alpha) \times g(\alpha)}{f(0.5) \times g(0.5)} = \left(\frac{T_\alpha}{T_{0.5}}\right)^2 \frac{\left(\frac{d\alpha}{dt}\right)_\alpha}{\left(\frac{d\alpha}{dt}\right)_{0.5}} \tag{11}$$

When the reaction reaches $\alpha = 0.5$, the temperature ($T_{0.5}$) and the conversion rate $(d\alpha/dt)_{0.5}$ are recorded.

The left side of Equation (11) represents a normalized theoretical curve for each reaction mechanism, expressed as $\frac{f(\alpha)\times g(\alpha)}{f(0.5)\times g(0.5)}$. Meanwhile, the right side of Equation (11) correlates with the experimental data at lower reaction rates, providing a basis for comparative analysis (Choudhary et al. 2024). The functional form of $f(\alpha)$ depends on the specific solid-state reaction mechanism, as detailed in Table 1.

Table 1. Various functions ($g(\alpha)$) of solid-state kinetic models: (1D: one-dimensional; 2D: two-dimensional; 3D: three-dimensional).

No.	Code	$g(\alpha)$	$f(\alpha)$	Rate-determining reaction mechanism
1. Chemical processes (CPs) or mechanisms that do not involve mathematical equations				
1	CP1	$1-(1-\alpha)^{2/3}$	$3/2(1-\alpha)^{1/3}$	Chemical reaction
2	CP2	$1-(1-\alpha)^{1/4}$	$4(1-\alpha)^{3/4}$	
3	CP3	$(1-\alpha)^{-1/2}-1$	$2(1-\alpha)^{3/2}$	
4	CP4	$(1-\alpha)^{-1}-1$	$(1-\alpha)^{2}$	
5	CP5	$(1-\alpha)^{-2}-1$	$1/2(1-\alpha)^{3}$	
6	CP6	$(1-\alpha)^{-3}-1$	$1/3(1-\alpha)^{4}$	
7	CP7	$1-(1-\alpha)^{2}$	$1/2(1-\alpha)$	
8	CP8	$1-(1-\alpha)^{3}$	$1/3(1-\alpha)^{2}$	
9	CP9	$1-(1-\alpha)^{4}$	$1/4(1-\alpha)^{3}$	
2. Acceleratory rate (AR) equations				
10	AR1	$\alpha^{3/2}$	$2/3\alpha^{-1/2}$	Nucleation
11	AR2	$\alpha^{1/2}$	$2\alpha^{1/2}$	
12	AR3	$\alpha^{1/3}$	$3\alpha^{2/3}$	
13	AR4	$\alpha^{1/4}$	$4\alpha^{3/4}$	
14	AR5	$\ln\alpha$	α	
3. Sigmoidal rate (SR) equations describe random nucleation followed by subsequent growth				
15	SR1	$-\ln(1-\alpha)$	$1-\alpha$	Assumed random nucleation and its subsequent growth
16	SR2	$[-\ln(1-\alpha)]^{2/3}$	$3/2(1-\alpha)[-\ln(1-\alpha)]^{1/3}$	
17	SR3	$[-\ln(1-\alpha)]^{1/2}$	$2(1-\alpha)[-\ln(1-\alpha)]^{1/2}$	
18	SR4	$[-\ln(1-\alpha)]^{1/3}$	$3(1-\alpha)[-\ln(1-\alpha)]^{2/3}$	
19	SR5	$[-\ln(1-\alpha)]^{1/4}$	$4(1-\alpha)[-\ln(1-\alpha)]^{3/4}$	
20	SR6	$[-\ln(1-\alpha)]^{2}$	$1/2(1-\alpha)[-\ln(1-\alpha)]^{-1}$	
21	SR7	$[-\ln(1-\alpha)]^{3}$	$1/3(1-\alpha)[-\ln(1-\alpha)]^{-2}$	
22	SR8	$[-\ln(1-\alpha)]^{4}$	$1/4(1-\alpha)[-\ln(1-\alpha)]^{-3}$	
23	SR9	$\ln\alpha/(1-\alpha)$	$\alpha/(1-\alpha)$	Branching nuclei
4. Deceleratory rate equations				
4.1. Phase boundary (PR) reaction				
24	PR1	α	1	Contracting disk
25	PR2	$1-(1-\alpha)^{1/2}$	$2(1-\alpha)^{1/2}$	Contracting cylinder (cylindrical symmetry)
26	PR3	$1-(1-\alpha)^{1/3}$	$3(1-\alpha)^{2/3}$	Contracting sphere (spherical symmetry)
4.2. Based on the diffusion mechanism (DM)				
27	DM1	α^{2}	$1/2\alpha$	1D diffusion
28	DM2	$\left[1-(1-\alpha)^{1/2}\right]^{1/2}$	$4\left\{(1-\alpha)[1-(1-\alpha)]^{1/2}\right\}^{1/2}$	2D diffusion
29	DM3	$\alpha+(1-\alpha)\ln(1-\alpha)$	$[-\ln(1-\alpha)]^{-1}$	
30	DM4	$\left[1-(1-\alpha)^{1/3}\right]^{2}$	$(3/2)(1-\alpha)^{2/3}\left[1-(1-\alpha)^{1/3}\right]^{-1}$	3D diffusion, spherical symmetry
31	DM5	$1-2/3\alpha-(1-\alpha)^{2/3}$	$(3/2)\left[(1-\alpha)^{-1/3}-1\right]^{-1}$	3D diffusion, cylindrical symmetry
32	DM6	$\left[(1-\alpha)^{-1/3}-1\right]^{2}$	$(3/2)(1-\alpha)^{4/3}\left[(1-\alpha)^{-1/3}-1\right]^{-1}$	3D diffusion
33	DM7	$\left[(1+\alpha)^{1/3}-1\right]^{2}$	$(3/2)(1+\alpha)^{2/3}\left[(1+\alpha)^{1/3}-1\right]^{-1}$	
34	DM8	$1+2/3\alpha-(1+\alpha)^{2/3}$	$(3/2)\left[(1+\alpha)^{-1/3}-1\right]^{-1}$	
35	DM9	$\left[(1+\alpha)^{-1/3}-1\right]^{2}$	$(3/2)(1+\alpha)^{4/3}\left[(1+\alpha)^{-1/3}-1\right]^{-1}$	
36	DM10	$\left[1-(1-\alpha)^{1/3}\right]^{1/2}$	$6(1-\alpha)^{2/3}\left[1-(1-\alpha)^{1/3}\right]^{1/2}$	

Results and discussion

Physicochemical properties of SrWRFs

Table 3 presents the key characteristics of *Syagrus romanzoffiana* waste rachis fibers (*Sr*WRFs). The analysis reveals favorable properties for thermal conversion processes, with low moisture (8.65%) and ash (1.03%) contents, moderate fixed carbon (7.97%), and a high volatile matter content (82.34%). These compositional features suggest *Sr*WRFs are particularly suitable for thermochemical applications such as pyrolysis, gasification, and combustion, where high volatile content and low inorganic impurities are advantageous (Pal et al. 2021). Other common lignocellulosic biomasses, like macadamia nut shells (67.39%) (Y. Wang et al. 2024b),

Table 2. The physicochemical properties of *Sr*.WRFs.

Analysis	Properties	Values
Ultimate analysis (wt.%)[a]	C	45.22
	H	5.51
	O	44.32
	N	0.78
	S	0.34
Proximate analysis (wt.%)[a]	Moisture[b]	8.65
	Ash	1.03
	Volatile fraction	82.34
	Fixed Carbon[b]	7.97
Compositional analysis (wt.%)[a]	Cellulose	47.36
	Hemicellulose	15.21
	Lignin	36.84
O to C ratio and H to C ratio[c]	O/C	0.74
	H/C	1.46
Molecular Formula	$CH_{1.46}\ O_{0.74}\ N_{0.015}\ S_{0.0028}$	–
Calorific Value (MJ/kg)	Higher heating value (HHV)[d]	18.42

[a]Dry basis.
[b]Air dry basis.
[c]Molar ratio.
[d]HHV = 0.3984 C +0.4030 H − 0.03153 O − 1.8644S + 0.2791 N (Ozyuguran, Akturk, and Yaman 2018).

Table 3. Thermogravimetric data for *Syagrus romanzoffiana* fibers. (T_i: initial decomposition temperature, T_f : final decomposition temperature, WL: weight loss, β: heating rate).

β (°C/min)	Specimen weight (mg)	T_i (°C)	T_f (°C)	T_m (°C)	WL (%)
30	6.00433	210	385	327	62.13
40	6.04431	232	415	361	63.31
50	6.1705	251	436	382	64.52

fodder radish seed cake (75.66%) (Silvestre, Pauletti, and Baldasso 2020), little millet (68.33%) (Mishra et al. 2023), and tobacco straw (78.25%) (Y. Wang et al. 2023a), do not have as much volatile matter (82.34%) as *Sr*WRFs. The high volatile content in *Sr*WRFs enhances their potential for bio-oil generation during thermal processing (M. Kumar et al. 2021). Elemental analysis revealed a composition of 45.22% carbon, 5.51% hydrogen, 44.32% oxygen, 0.78% nitrogen, and 0.34% sulfur. This favorable elemental distribution, particularly the low nitrogen and sulfur percentages, indicates that *Sr*WRFs would likely produce minimal toxic emissions when subjected to thermal decomposition processes (Ahmad et al. 2017). The chemical composition of *SrWRF*s is represented by the formula $CH_{1.46}\ O_{0.74}\ N_{0.015}\ S_{0.0028}$. Research suggests that a higher hydrogen-to-carbon (H/C) ratio coupled with a lower oxygen-to-carbon (O/C) ratio can improve the quality of bio-oil, making it more suitable as a fuel source (M. Kumar et al. 2021; Silvestre, Pauletti, and Baldasso 2020). The H/C ratio (1.46) is greater than that of peanut shells (0.88) (M. Kumar et al. 2021), ginkgo (1.22) (L. Wang et al. 2018), poplar (1.18) (L. Wang et al. 2018), and wheat straw lignin (1.23) (L. Wang et al. 2018), and the O/C ratio (0.74) is less than that of *Imperata cylindrica* (0.83) (S. Hidayat, M. S. A. Bakar, A. Ahmed, D. A. Iryani, M. Hussain, F. Jamil, and Y. K. Park 2021), sugarcane bagasse (0.82) (L. Wang et al. 2018), and pineapple peel waste (0.97) (da Silva et al. 2022), suggesting an increased potential as an energy source. With a heating value (HHV) of 18.42 MJ/kg, *Sr*WRFs are superior to a variety of common lignocellulosic biomass sources, including macadamia nut shells (18.19 MJ/kg) (Y. Wang et al. 2024b), sunflower stalks (14.78 MJ/kg) (Mishra et al. 2023), grape marc (17.37 MJ/kg) (Fernandez et al. 2023a), Rosa rubiginosa L. waste (16.96 ± 0.17 MJ/kg) (Torres-Sciancalepore et al. 2023), and Syzygium jambolana seeds (14.20 MJ/kg) (Pal et al. 2021). This means that *Sr*WRFs are perfect as a raw material for pyrolysis and combustion processes. *Sr*WRFs were found to include hemicellulose (15.21%), cellulose (47.36%), and a large amount of lignin (36.84%). The lignin concentration (36.84%) is greater than that of peanut shells (19.55%) (M. Kumar et al. 2021), macadamia nut shells (15.58%) (Y. Wang et al. 2024b), and pinewood sawdust (25.6%) (J. Wang et al. 2022), which explains *Sr*WRFs' high calorific value and mechanical strength (Umezawa 2018).

Thermogravimetric analysis (TGA) of Syagrus romanzoffiana waste rachis fibers (SrWRFs)

The TG and derivative thermogravimetry (DTG) plots of *Sr*WRFs in Figure 2, analyzed at β values of 30, 40, and 50°C/min, exhibited consistent trends while shifting toward higher temperatures as β increased. This shift, attributed to delayed heat and mass transfer (Naqvi, Hameed, et al. 2019), resulted in a temperature hysteresis effect, causing the TG WL curve to move laterally without changing the decomposition behavior. Higher β also resulted in slower reactions and broader DTG peaks, indicating delayed sample

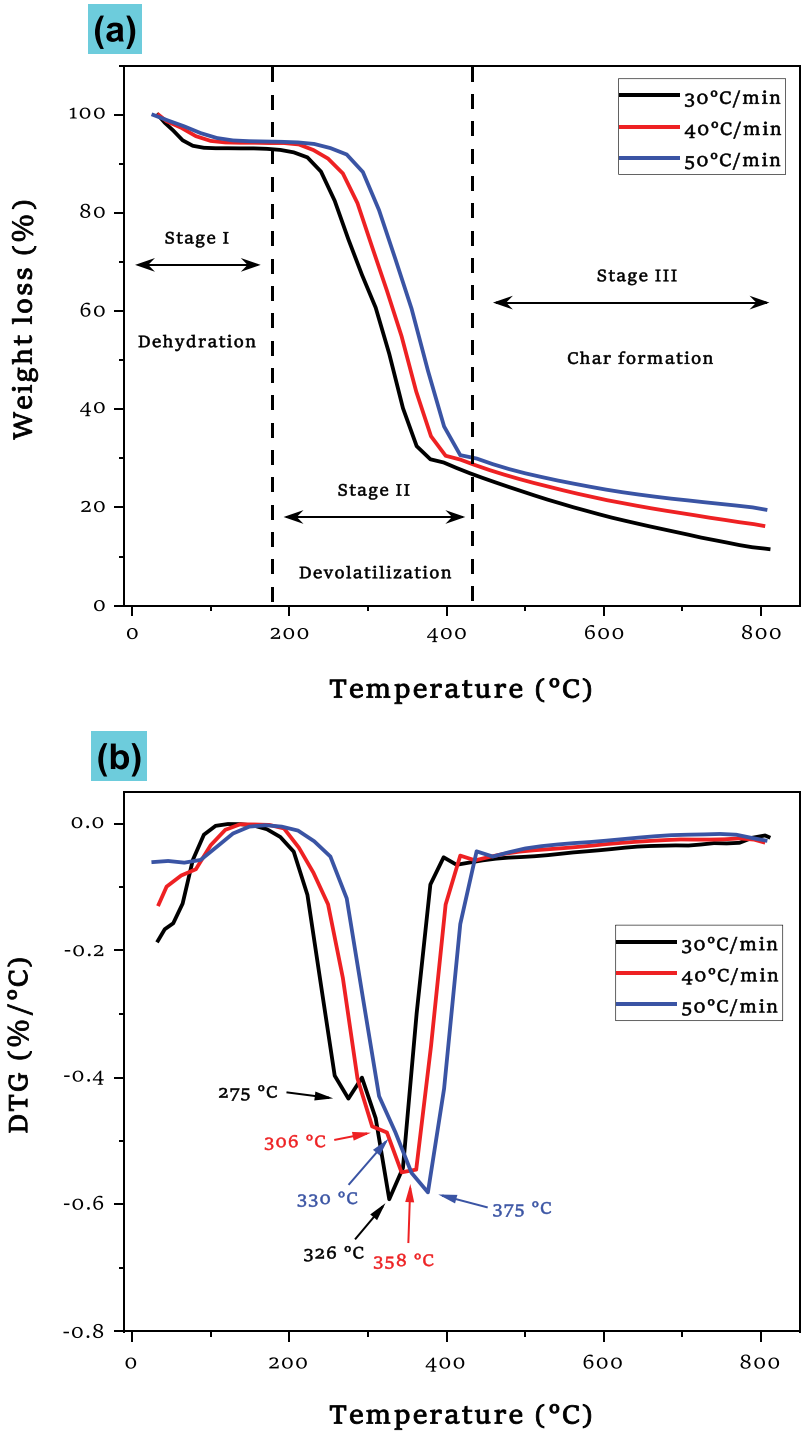

Figure 2. (a) Thermogravimetric analysis (TGA) and (b) derivative thermogravimetric (DTG) profiles of *Syagrus romanzoffiana* waste rachis fibers (*Sr*WRFs) at various heating rates (30, 40, and 50°C/min).

decomposition due to inadequate internal heating (Zhao, Jiang, and Chen 2017). Thus, the increased β value delays thermal degradation without altering the fundamental decomposition mechanism.

Table 3 displays TG-DTG data at β values of 30, 40, and 50°C/min, indicating a shift toward higher decomposition temperatures, while WL remained approximately constant at 60% during active pyrolysis. The DTG profiles revealed overlapping reactions in this zone, indicating the breakdown of thermally stable components (M. Ali et al. 2021). Despite variations in β, the volatile release and WL patterns remained consistent, indicating stable pyrolysis behavior under the tested conditions.

Determining pyrolysis characteristic parameters – such as the initial decomposition temperature (T_i), peak decomposition temperature (T_p), final decomposition temperature (T_f), and weight loss (WL) – is critical for optimizing thermochemical conversion processes like pyrolysis and gasification (Chen, Li, Zhang, et al. 2019; Z. Huang et al. 2015a). These parameters reveal how biomass behaves under thermal treatment, guiding reactor design, temperature settings, and residence times to maximize volatile yields and minimize char formation (Lei et al. 2023; Mishra et al. 2023). By understanding T_i (indicating activation energy), T_p (reflecting maximum decomposition rate), and T_f (marking reaction completion), engineers can tailor processes to specific feedstocks, enhancing energy efficiency and sustainability. Ignoring these parameters would hinder the ability to predict product distribution, reduce waste, and improve the economic viability of biomass utilization, which is why their determination and explanation are essential (Hadou et al. 2024b).

The thermal degradation of *Sr*WRFs exhibited clear decomposition stages, consistent with prior research (Fernandez et al. 2017), beginning with moisture evaporation followed by sequential breakdown of HCL, CL, and LG. The study precisely determined the onset and completion temperatures for each degradation phase in *Sr*WRFs, confirming similar decomposition kinetics to biomass materials.

The thermal decomposition of *Sr*WRFs occurred in four distinct stages:

- First Stage (Moisture Evaporation): Occurred from ambient temperature to approximately 130°C, marking the drying phase.
- Second Stage – Part 1 (HCL Degradation): Spanned from 180°C to 300°C, corresponding to typical HCL breakdown in biomass.
- Second Stage – Part 2 (CL Degradation): Took place between 300°C and 400°C, indicating CL's primary decomposition.
- Third Stage (LG Degradation): Extended from 400°C to 800°C, capturing the complex, multi-step degradation of LG.

The DTG curves displayed a broad peak with lower-temperature shoulders across all β values, resulting from the overlapping decomposition of the biomass P-components (Fernandez et al. 2023b). Increased β values caused the DTG peaks to shift to higher temperatures, resulting from shorter reaction times.

Figure 3 illustrates the evolution of α and $d\alpha/dT$ as a function of T at β values of 30, 40, and 50°C/min. While the curve shapes largely remain consistent, they shift toward wider temperature ranges as β increases. This temperature hysteresis effect arises because the sample's thermal response lags behind the programmed β (Yao et al. 2008). The hysteresis becomes more pronounced at higher β. Significantly, the maximum and mean $d\alpha/dT$ values show minimal dependence on β, as the counteracting effects of increasing temperature (which raises $d\alpha/dT$) and quicker heating (which reduces $d\alpha/dT$) nearly offset each other. The temperature at which peak $d\alpha/dT$ occurs systematically increases with β, in line with the expectations of kinetic theory (Poletto, Ornaghi Jnior, and Zattera 2015).

Three-parallel Gaussian reaction model analysis of Syagrus romanzoffiana waste rachis fibers (SrWRFs)

This study aimed to develop a three-parallel Gaussian reaction model based on the primary decomposition stage (i.e., Stage II, 200–650°C) by utilizing $d\alpha/dT$ profiles (Figure 3). Figure 4 illustrates that the model was created to elucidate the complex pyrolysis behavior of the three primary biomass components. Component-specific pyrolysis intervals were defined based on their characteristic peak temperatures (T_p), following the established trend of thermal stability: HCL (lowest T_p) < CL < LG (highest T_p) (S. Hidayat, Bakar, Ahmed,

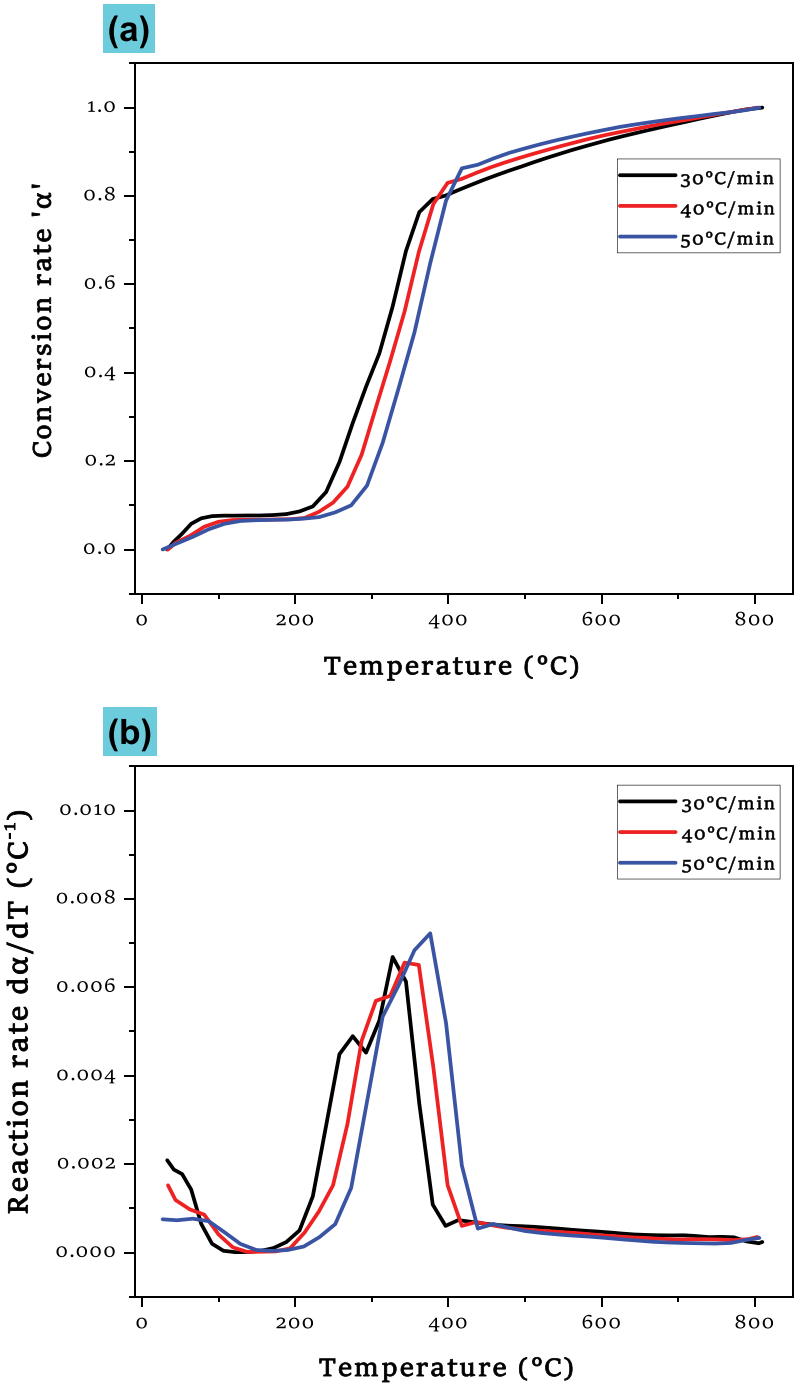

Figure 3. (a) Conversion rate (*a*) for the pyrolysis of *Syagrus romanzoffiana* waste rachis fibers (*Sr*WRFs), and (b) reaction rate (d*a*/d*T*) at 30, 40, and 50°C/min.

Iryani, Hussain, Jamil, and Park 2021). These reference peaks (P-HCL, P-CL, and P-LG) served as essential alignment markers for the Gaussian reaction model. The decomposition stage was successfully divided into three distinct phases, each demonstrating excellent fitting accuracy ($R^2 \geq 0.99537$), confirming the model's ability to accurately represent the overlapping decomposition processes through parallel Gaussian reactions.

The three-parallel Gaussian reaction model effectively characterizes the primary pyrolysis stage (i.e., Stage II, 200–650°C) of *Sr*WRFs, demonstrating excellent fitting accuracy ($R^2 \geq 0.99537$). The model's reliability arises from the consistent trend of thermal stability ($T_{P\text{-}HCL} < T_{P\text{-}CL} < T_{P\text{-}LG}$), which accurately delineates the decomposition ranges for each biomass component. Remarkably, the determined temperature intervals for P-components (HCL: 200–345°C, CL: 305–398°C, LG: 220–650°C) remained stable across various heating

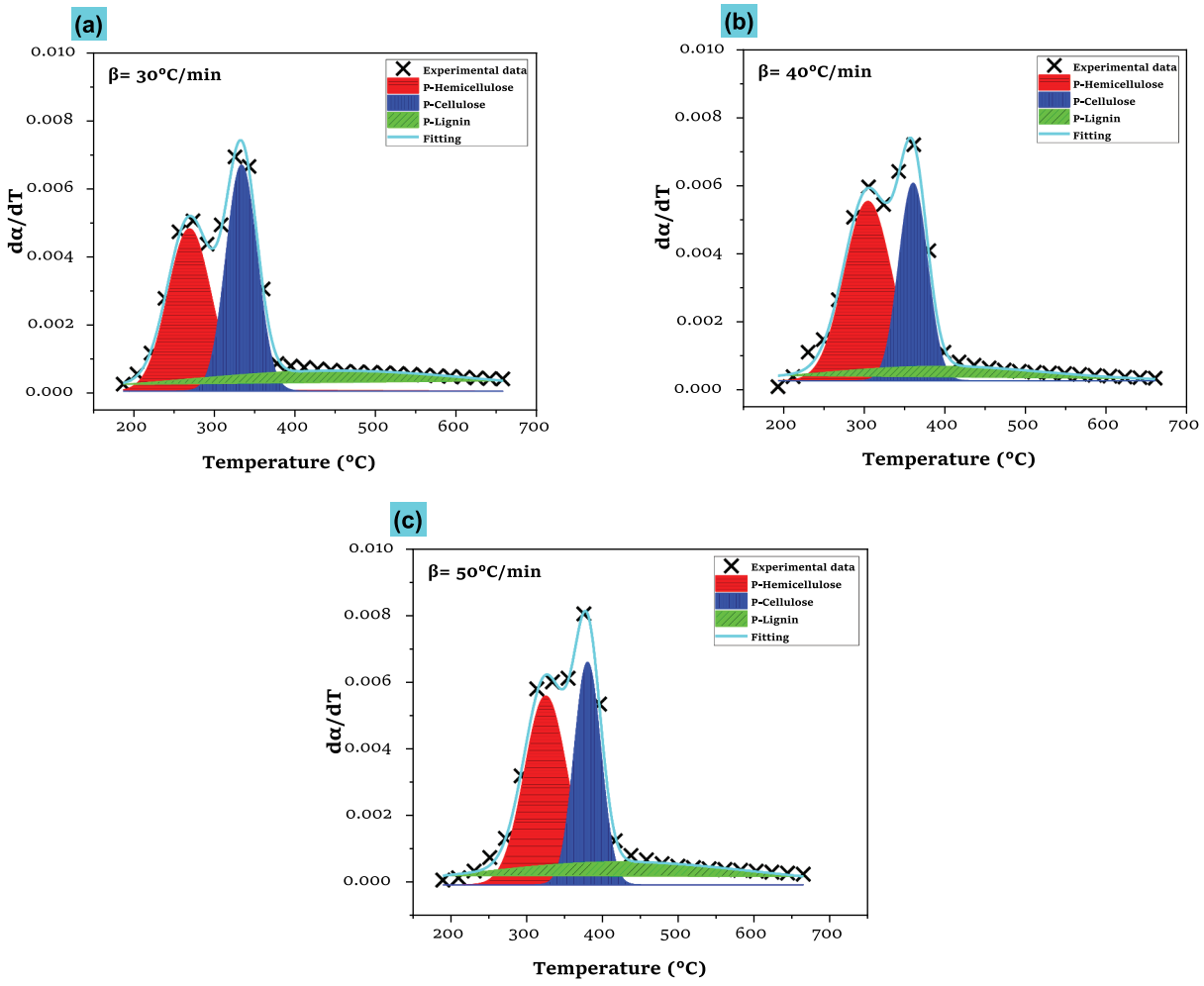

Figure 4. Results of deconvolution for the second stage of dα/dT of *Syagrus romanzoffiana* waste rachis fibers (*Sr*WRFs) at three heating rates (β), using the four-parallel Gaussian kinetic model.

rates (β: 30–50°C/min) and were consistent with literature values (Ma et al. 2023; Y. Wang et al. 2023b), validating the model's accuracy. The strong correlation between these intervals and established decomposition characteristics further supports the model's robustness. With its strong correlation coefficients and consistent performance under various experimental conditions, this model demonstrates its value in predicting pyrolysis behavior across diverse applications (Y. Wang et al. 2023b, 2024c).

Table 4 shows the Gaussian decomposition parameters for HCL (P-HCL), CL (P-CL), and LG (P-LG) at a β of 30, 40, and 50°C/min. The model identified distinct thermal decomposition ranges: 204–345°C for

Table 4. Gaussian parameters for pseudo-components (P-components): pseudo-hemicellulose (P-HCL), pseudo-cellulose (P-CL), and pseudo-lignin (P-LG).

P-component		30°C/min	40°C/min	50°C/min
P-HCL	y_0	4.44×10^{-5}	2.51×10^{-4}	-7.61×10^{-5}
	x_c	270.59	304.65	325.94
	A	0.3159	0.3833	0.3946
	w	62.26	68.31	65.41
	RMSE	0.028	0.034	0.036
P-CL	x_c	335.16	360.61	381.11
	A	0.3171	0.2547	0.2923
	w	44.88	41.23	41.12
	RMSE	0.032	0.029	0.031
P-LG	x_c	452.87	387.94	423.01
	A	0.2667	0.1451	0.2981
	w	417.65	311.98	404.70
	RMSE	0.041	0.040	0.039

HCL, 305–398°C for CL, and 220–650°C for LG, which align with the literature-reported intervals of 203–464°C (HCL), 302–387°C (CL), and 127–791°C (LG) (W.-H. Chen et al. 2020; Zong et al. 2020). These results confirm a firm consistency with previous studies, validating the accuracy of the three-parallel reaction model. The observed thermal stability sequence (CL < HCL < LG) confirms that LG has a characteristically broad decomposition range, as noted in reference (S. Hidayat, Bakar, Ahmed, Iryani, Hussain, Jamil, and Park 2021).

To comprehensively assess the precision of the three-parallel Gaussian model for deconvoluting *SrWRFs'* DTG profiles, residual and error analyses were performed alongside correlation coefficients (Figure 5). Residuals displayed a tight, random distribution around zero across all heating rates (30, 40, and 50°C/min), with no systematic bias, indicating that the model accurately captures overlapping hemicellulose, cellulose, and lignin decomposition processes without consistently over- or underestimating trends. Slight deviations near hemicellulose and lignin peak shoulders, likely due to experimental noise and baseline artifacts, align with known challenges in high-β thermogravimetry (Fischer, Lemaire, and Bensakhria 2024; Najafi, Rezaei Laye, and Sobati 2024). The model's accuracy was further validated by low root mean square error (RMSE) values across all pseudo-components and heating rates (Table 4), with RMSE at 30°C/min being 0.032%/min for P-HCL, 0.028%/min for P-CL, and 0.041%/min for P-LG; at 40°C/min, 0.034, 0.029, and 0.040%/min; and at 50°C/min, 0.036, 0.031, and 0.039%/min, respectively (all <0.05%/min). These minimal errors, combined with high R^2 values (≥0.99537), confirm negligible fitting errors and robust Gaussian deconvolution. Recent biomass pyrolysis studies, including (Arumugam and Ganesan 2024; Bongomin et al. 2024; Fischer, Lemaire, and Bensakhria 2024; Lalaymia et al. 2024), and (Choudhary et al. 2024) emphasize the combined use of R^2, residual distribution, and RMSE to ensure reliable model fits, preventing overreliance on correlation coefficients and aligning with contemporary kinetic modeling standards for lignocellulosics.

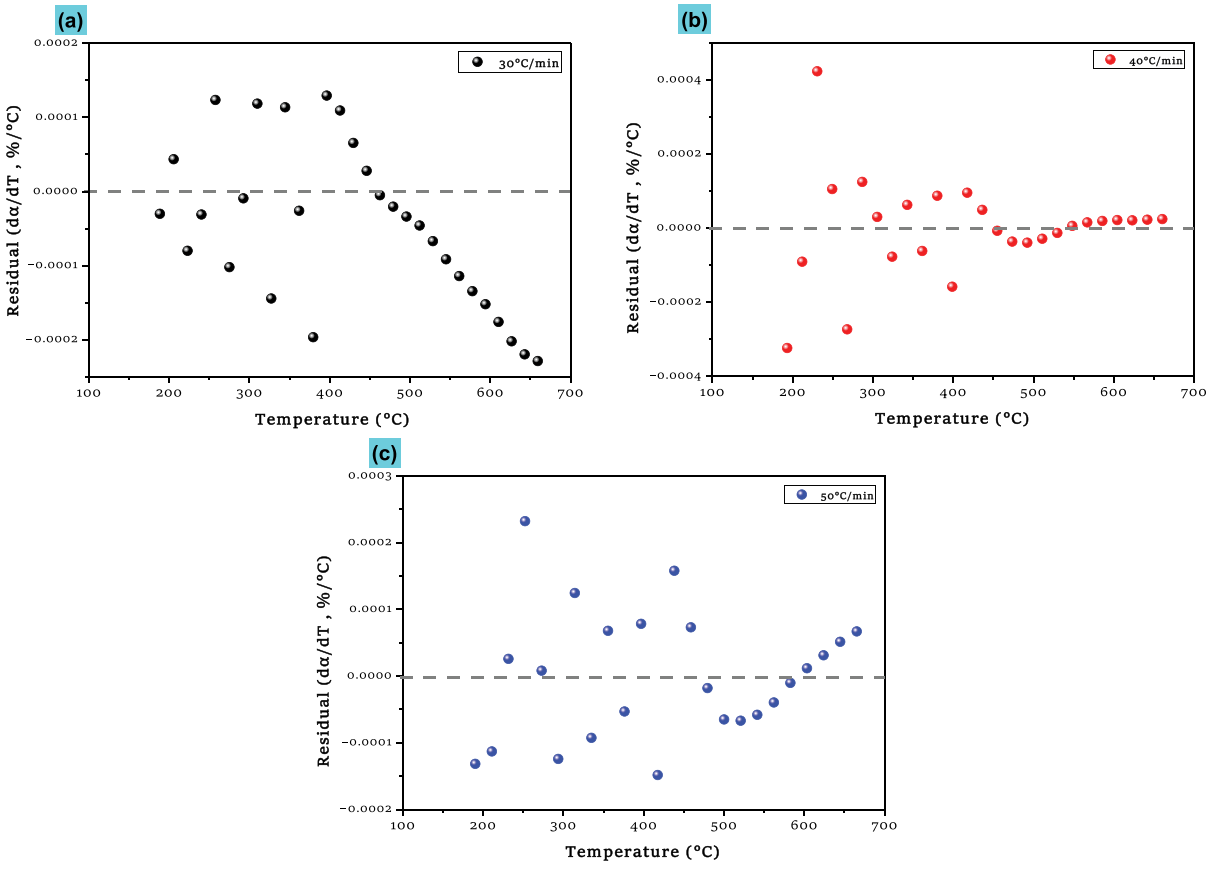

Figure 5. Residual plots of the three-parallel Gaussian model fits at heating rates of 30, 40, and 50°C/min.

Although no direct spectroscopic validation was performed, the thermal peak assignments are consistent with decomposition intervals extensively reported in lignocellulosic literature, supporting their reliability within the scope of this kinetic modeling approach.

Kinetic investigation of Syagrus romanzoffiana waste rachis fibers (SrWRFs)

The kinetic parameters obtained for *Sr*WRF pyrolysis, as determined by the CRM, are summarized in Table 5 and compared with those from earlier studies in Table 6. The analysis revealed an E_a ranging from 203.98 to 262.11 kJ/mol and an A between 1.18×10^{17} and 1.01×10^{22} min^{-1} for the reaction model $[-\ln(1-\alpha)]^4$. These values are significantly higher than those reported for other biomass materials, including surgical face masks (237.19 kJ/mol), pine and corn starch pellets (218.05 kJ/mol), and chicken waste (140.4–151.2 kJ/mol), as shown in Table 6. This notable difference highlights the distinct thermal degradation behavior of *Sr*WRFs, which necessitates a higher energy input due to their complex composition and structural properties.

The CRM analysis revealed strong correlation coefficients (R^2) across all tested kinetic models, including chemical reaction models, SR equations for nucleation-growth mechanisms, and deceleratory rate equations at various β values (30–50°C/min). Models CP3, CP4, CP5, SR6, SR7, SR8, and DM6 exhibited excellent fits

Table 5. Activation energy (E_a) and pre-exponential factor (ln$A$) of *Syagrus romanzoffiana* waste rachis fibers (*Sr*WRFs) calculated using the Coats–Redfern method (CRM) at heating rates (β) of 30, 40, and 50°C/min.

	β of 30°C/min			β of 40°C/min			β of 50°C/min		
Code	E_a (kJ/mol)	R^2	ln$A$ (min^{-1})	E_a (kJ/mol)	R^2	ln$A$ (min^{-1})	E_a (kJ/mol)	R^2	ln$A$ (min^{-1})
1. Chemical processes (CPs) or mechanisms that do not involve equations									
CP1	38.58	0.982	5.49	40.85	0.985	6.07	47.25	0.989	7.52
CP2	41.89	0.987	6.16	47.39	0.994	7.44	53.73	0.991	8.83
CP3	48.36	0.991	7.49	61.21	0.995	10.32	67.39	0.981	11.57
CP4	53.03	0.992	8.44	71.84	0.989	12.54	77.89	0.968	13.68
CP5	63.18	0.991	10.52	96.15	0.969	17.62	101.85	0.936	18.49
CP6	74.36	0.987	12.80	123.67	0.949	23.37	101.85	0.907	18.49
CP7	29.26	0.959	3.58	24.82	0.904	2.72	31.30	0.944	4.32
CP8	23.48	0.929	2.40	16.68	0.789	1.02	23.04	0.879	2.66
CP9	18.61	0.886	1.40	10.81	0.623	−0.20	16.90	0.793	1.43
2. Acceleratory rate (AR) equations									
AR1	58.78	0.982	9.62	59.20	0.977	9.90	68.95	0.986	11.88
AR2	13.36	0.959	0.33	13.15	0.945	0.28	16.29	0.970	1.31
AR3	5.79	0.902	−1.22	5.47	0.860	−1.32	7.51	0.935	−0.45
AR4	2.00	0.648	−2.00	1.64	0.476	−2.12	3.12	0.807	−1.34
AR5	–	–	–	–	–	–	–	–	–
3. Sigmoidal rate (SR) equations describe random nucleation followed by subsequent growth									
SR1	43.98	0.988	6.59	51.71	0.996	8.34	57.99	0.989	9.68
SR2	26.20	0.985	2.95	31.18	0.995	4.05	35.32	0.987	5.13
SR3	17.31	0.981	1.13	20.92	0.993	1.91	23.98	0.985	2.85
SR4	8.42	0.963	−0.68	10.65	0.988	−0.24	12.64	0.977	0.58
SR5	3.98	0.907	−1.59	5.52	0.973	−1.31	6.97	0.961	−0.56
SR6	97.31	0.991	17.50	113.29	0.997	21.20	126.03	0.991	23.34
SR7	150.64	0.991	28.41	174.87	0.997	34.06	194.07	0.991	37.01
SR8	203.98	0.992	39.31	236.45	0.997	46.92	262.11	0.991	50.67
SR9	–	–	–	–	–	–	–	–	–
4. Deceleratory rate equations									
4.1. Phase boundary (PR) reaction									
PR1	36.07	0.978	4.97	36.18	0.972	5.09	42.62	0.983	6.60
PR2	39.88	0.984	5.75	43.37	0.989	6.60	49.75	0.990	8.03
PR3	41.22	0.986	6.03	46.02	0.992	7.15	52.37	0.991	8.55
4.2 Based on the diffusion mechanism (DM)									
DM1	81.49	0.983	14.26	82.23	0.979	14.71	95.28	0.987	17.17
DM2	15.26	0.972	0.72	16.75	0.980	1.04	19.85	0.985	2.02
DM3	86.40	0.986	15.27	91.16	0.988	16.58	104.15	0.991	18.95
DM4	91.78	0.989	16.37	101.92	0.994	18.83	114.79	0.992	21.09
DM5	88.19	0.987	15.63	94.72	0.990	17.32	107.66	0.992	19.65
DM6	103.09	0.992	18.68	125.70	0.997	23.79	138.30	0.986	25.81
DM7	75.21	0.980	12.98	73.50	0.972	12.89	86.31	0.983	15.37
DM8	77.25	0.981	13.39	76.30	0.975	13.47	89.20	0.984	15.95
DM9	69.27	0.976	11.76	65.40	0.963	11.20	77.96	0.977	13.69
DM10	15.93	0.975	0.85	18.07	0.986	1.31	21.16	0.986	2.29

Table 6. Comparison of kinetic parameters between this study and other biomass-based material, including waste fibers, seeds, pellets, and residues.

Specimen	β (°C/min)	E_a (kJ/mol)	A (min^{-1})	Reaction model $g(\alpha)$	Ref.
*Sr*WRFs	30, 40, and 50	203.98 to 262.11	1.18×10^{17} to 1.01×10^{22}	$[-\ln(1-\alpha)]^4$	Current study
Surgical face mask	15, 20, 25, 30	237.19	1.36×10^{14}	$[-\ln(1-\alpha)]^{2/3}$	S. Sun et al. (2021)
Pine and corn starch pellet	5, 10, 20, and 50	218.05	1.28×10^{14}	$1-(1-\alpha)^{1/3}$	Tabal et al. (2021)
Date seeds	10, 20, 30, and 40	170–190	13.8×10^{12}	$\left[(1-\alpha)^{-1/3}-1\right]^2$	Raza, Abu-Jdayil, and Inayat (2023)
Chicken waste	10, 15, 25	140.4–151.2	2.91×10^9 to 4×10^{10}	$[1/(1-\alpha)]-1$	Zikhali et al. (2023)
Flower stalk of *Agave americana*	5, 10, and 20	88.818	179.56	$\alpha+(1-\alpha)ln(1-\alpha)$	Lalaymia et al. (2024)
Dracaena draco fibers	5, 10, and 20	87.58	1.62×10^5	$[-\ln(1-\alpha)]^4$	Hadou et al. (2024b)

($R^2 \geq 0.99$) at 30°C/min, while additional models (CP2, CP3, SR1, SR2, SR3, SR6, SR7, SR8, PR3, DM4, DM5, and DM6) demonstrated strong performance at 40°C/min. At the highest β value (50°C/min), models CP2, SR6, SR7, SR8, PR2, PR3, DM3, DM4, and DM5 indicated strong correlations; however, some models displayed weaker fits. These results illustrate that the applicability of kinetic models is influenced by β, with certain models consistently performing well under all conditions, thereby highlighting their robustness in capturing the complex pyrolysis behavior of *Sr*WRFs.

Table 5 presents E_a and ln$A$ derived from the CRM for the pyrolysis of *Sr*WRFs at β values of 30, 40, and 50°C/min, highlighting the minimum energy needed to initiate the release of volatiles during thermal decomposition (Sobek and Werle 2020). The kinetic analysis focused on the active pyrolysis range (200–-650°C), which is believed to follow a single-step degradation mechanism, and evaluated 36 solid-state reaction models, including chemical, nucleation-growth, and diffusion models (M. Kumar, Mishra, and Upadhyay 2020). Elevated E_a values indicate that the reaction demands higher temperatures and longer durations to overcome the energy barriers for complete breakdown (Naqvi et al. 2020).

All models exhibited strong correlation coefficients (R^2), with the diffusional models (SR6, SR7, and SR8) displaying exceptional fits ($R^2 \geq 0.99$) across all β values. The superior performance of these models likely results from their ability to capture diffusion-controlled volatile release, a dominant phenomenon in biomass decomposition (Wu et al. 2022). The studied samples showed significant variations in E_a, underscoring differences in their thermal degradation behavior (Rasam et al. 2020), while the consistency of diffusional models confirms their reliability in predicting *Sr*WRF pyrolysis kinetics (Wu et al. 2022).

Figure 6 illustrates the best-fitting models for Area I at β values of 30, 40, and 50°C/min, while Table 5 summarizes the kinetic parameters obtained from the CRM analysis. Among the models tested, only the SR equations (SR6, SR7, and SR8), which represent random nucleation and growth mechanisms, consistently achieved high correlation coefficients ($R^2 \geq 0.99$) across all β values. The SR6 model yielded E_a values of 97.31, 113.29, and 126.03 kJ/mol at β of 30, 40, and 50°C/min, respectively. Similarly, SR7 yielded E_a values of 150.64, 174.87, and 194.07 kJ/mol, while SR8 produced higher values of 203.98, 236.45, and 262.11 kJ/mol (Figures 6(a-c)). Overall, the mean E_a range for *Sr*WRFs, based on these optimal models, varied from 97.31 to 262.11 kJ/mol.

The kinetic compensation effect (KCE), a comprehensive phenomenon in the thermal analysis literature (Chen, Li, Zhang, et al. 2019; Jiang et al. 2018; Vyazovkin et al. 2011), describes the linear interdependence between E_a and the natural logarithm of the pre-exponential factor (i.e., ln$A$). This relationship is mathematically represented as:

$$\ln A = a + b \times E_a \tag{12}$$

The coefficients a and b represent characteristic constants for a given kinetic dataset. Parameter a corresponds to the logarithmic transformation of the isokinetic rate parameter ($\ln k_{iso}$). In contrast, b is related to the inverse of the isokinetic temperature through Equation (13):

$$b = \frac{1}{RT_{iso}} \tag{13}$$

where: R is the universal gas constant and T_{iso} denotes the theoretical isokinetic temperature.

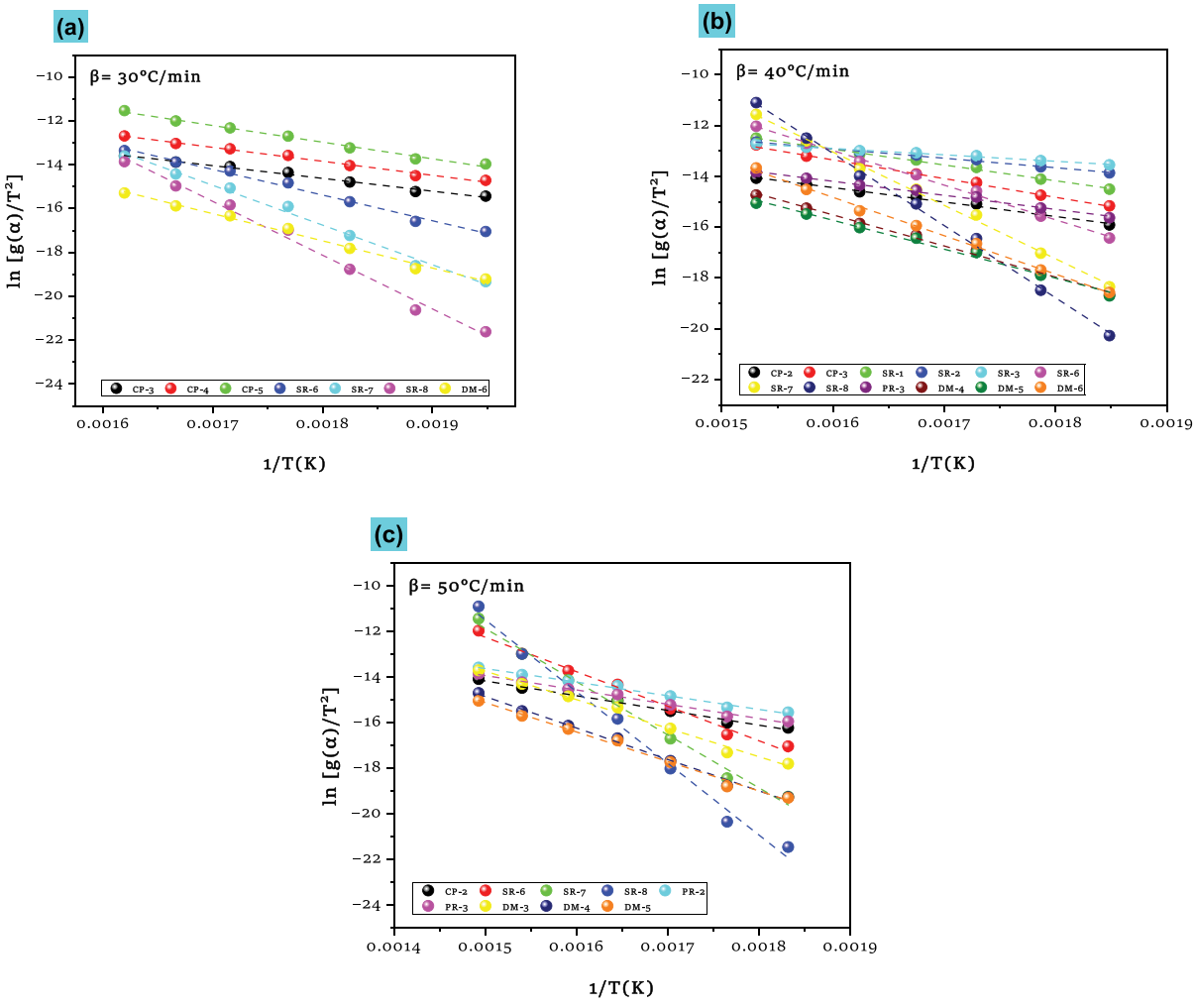

Figure 6. Model-fitting curves using integral methods to determine kinetic parameters for biomass pyrolysis, evaluated across various diffusion and reaction-order models.

Figure 7 illustrates this compensation effect by plotting ln$A$ against the E_a values obtained from CRM (Table 5). For a comprehensive characterization of the KCE, Table 7 provides detailed statistical parameters, including the compensation coefficients (a and b), their corresponding 95% confidence intervals, calculated isokinetic parameters (k_{iso} and T_{iso}), and the correlation coefficient (R^2), which quantifies the linearity of the relationship. This quantitative analysis confirms the strength of the compensation effect under diverse heating conditions, further validating its role in characterizing the pyrolysis kinetics of the materials studied. The strong correlations observed, typically with $R^2 > 0.95$ in most studies (Chen, Li, Zhang, et al. 2019; Vyazovkin et al. 2011), further validate the compensation effect as a fundamental characteristic of solid-state thermal decomposition processes.

Research indicates that the validity of the selected kinetic models for determining the kinetic triplet using the CRM can be verified when the calculated isokinetic temperature (T_{iso}) falls within the actual pyrolysis temperature range (Chen, Li, Zhang, et al. 2019; Jiang et al. 2018; Vyazovkin et al. 2011). As shown in Table 7, the derived T_{iso} values of 587.67°C (30°C/min), 575.45°C (40°C/min), and 598.50°C (50°C/min) all lie within the characteristic pyrolysis temperature range of *Sr*WRFs, as supported by the TG data in Figure 2. Additionally, the exceptionally high correlation coefficients ($R^2 > 0.98$) provide strong support for the model's validity. These findings collectively indicate that all 36 reaction models in Table 1 are statistically appropriate for determining the kinetic triplet using the CR approach.

The linear relationship mathematically represents the robust KCE observed across all β values:

$$\ln A = 0.2047E_a - 2.2836 \tag{14}$$

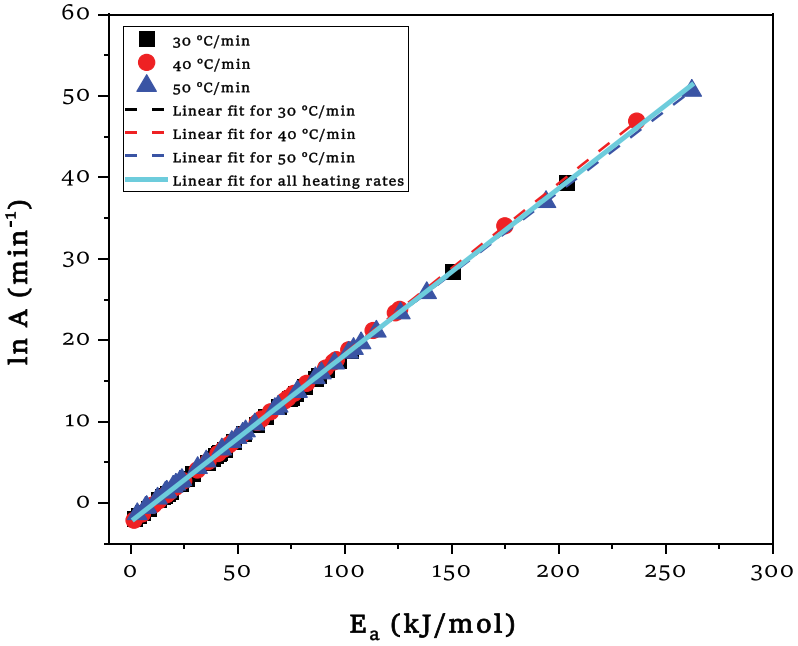

Figure 7. Isokinetic plots (ln*A vs.* E_a) for biomass pyrolysis based on the Coats–Redfern method (CRM) across various heating conditions.

Table 7. Kinetic compensation effect (KCE) parameters obtained from the Coats–Redfern method (CRM) at various heating rates (β of 30, 40, and 50°C/min).

β (°C/min)	A (min^{-1})	95% CI for a	b (mol/kJ)	95% CI for b	k_{iso}	T_{iso} (°C)	R^2
30	−2.4048	(−2.4056, −2.4039)	0.2045	(0.20449, 0.20453)	0.0903	587.67	0.99
40	−2.4619	(−2.4626, −2.4612)	0.20884	(0.20881, 0.20886)	0.0853	575.45	0.99
50	−1.9626	(−1.9635, −1.9617)	0.2008	(0.20078, 0.20082)	0.1405	598.50	0.99
Combination of all βs	−2.2836	(−2.3148, −2.2524)	0.2047	(0.20431, 0.20509)	0.1019	587.09	0.99

Equation (14) quantitatively demonstrates the essential interdependence between E_a and A, a hallmark of solid-state decomposition processes. The consistency of these parameters across various β values (30–50°C/min) further confirms the reliability of the selected models and the CR methodology for analyzing *Sr*WRF pyrolysis kinetics (Chen, Li, Xu, et al. 2019; Chen, Li, Zhang, et al., 2019; Jiang et al. 2018; Vyazovkin et al. 2011).

The observed kinetic compensation effect reflects the interdependence of E_a and A, likely arising from similar transition state structures across decomposition stages. This suggests a consistent energy barrier modulation mechanism despite varying β. However, the CMP approach, while useful, is limited at $\alpha > 0.55$ where experimental curves deviate from theoretical models, highlighting the need for hybrid kinetic approaches to fully resolve the reaction complexity (K. Sun et al. 2023).

Investigation of thermodynamic characteristics

Table 8 presents the thermodynamic parameters (ΔH, ΔG, and ΔS) that characterize the degradation of *Sr*WRFs at three different β values of 30, 40, and 50°C/min. The enthalpy change (ΔH), which represents the heat flux during the process at constant pressure (Z. Huang et al. 2015b), serves as a key indicator of reaction energetics. Negative ΔH values indicate exothermic processes that release energy, while positive ΔH values, as observed in this study, represent endothermic reactions that require external energy input to occur (L. Huang et al. 2016).

These thermodynamic measurements reveal fundamental principles governing the energy requirements and spontaneity of *Sr*WRF decomposition under various thermal conditions. Among the tested models, SR6, SR7, and SR8 exhibited the most consistent kinetic behavior, showing ΔH values of 94.59, 147.92, and

Table 8. Thermodynamic properties of *Syagrus romanzoffiana* waste rachis fibers (*Sr*WRFs) at different heating rates (β).

	β of 30°C/min			β of 40°C/min			β of 50°C/min		
Code	ΔH (kJ/mol)	ΔG (kJ/mol)	ΔS (kJ/mol.K)	ΔH (kJ/mol)	ΔG (kJ/mol)	ΔS (kJ/mol.K)	ΔH (kJ/mol)	ΔG (kJ/mol)	ΔS (kJ/mol.K)
1. Chemical processes (CPs) or mechanisms that do not involve equations									
CP1	35.86	114.71	−0.24	37.85	123.04	−0.24	44.07	130.35	−0.23
CP2	39.17	118.35	−0.24	44.39	127.71	−0.23	50.55	135.06	−0.22
CP3	45.64	118.40	−0.22	58.20	129.50	−0.20	64.21	136.42	−0.19
CP4	50.31	117.95	−0.21	68.84	130.54	−0.17	74.72	137.07	−0.16
CP5	60.46	119.27	−0.18	93.14	135.86	−0.12	98.67	141.61	−0.11
CP6	71.64	121.80	−0.15	120.67	143.30	−0.06	98.67	121.91	−0.06
CP7	26.54	109.17	−0.25	21.82	116.01	−0.26	28.12	123.31	−0.25
CP8	20.76	106.64	−0.26	13.68	113.44	−0.28	19.86	120.57	−0.26
CP9	15.89	104.81	−0.27	7.81	112.12	−0.29	13.72	118.90	−0.28
2. Acceleratory rate (AR) equations									
AR1	56.05	122.99	−0.20	56.20	129.67	−0.20	65.77	137.97	−0.19
AR2	10.64	104.18	−0.29	10.15	113.17	−0.29	13.11	119.48	−0.28
AR3	3.07	102.65	−0.30	2.47	112.30	−0.30	4.33	118.09	−0.30
AR4	−0.72	103.64	−0.32	−1.37	114.18	−0.32	−0.06	118.96	−0.31
AR5	–	–	–	–	–	–	–	–	–
3. Sigmoidal rate (SR) equations or random nucleation and subsequent growth									
SR1	41.26	115.19	−0.23	48.70	124.73	−0.21	54.82	131.75	−0.20
SR2	23.48	108.04	−0.26	28.17	117.52	−0.25	32.14	124.04	−0.24
SR3	14.59	104.89	−0.28	17.91	114.36	−0.27	20.80	120.63	−0.26
SR4	5.70	102.57	−0.30	7.65	112.02	−0.29	9.46	118.03	−0.28
SR5	1.26	102.47	−0.31	2.52	111.82	−0.30	3.79	117.60	−0.30
SR6	94.59	138.70	−0.13	110.28	148.55	−0.11	122.85	157.12	−0.09
SR7	147.92	163.18	−0.05	171.87	173.42	0.00	190.89	183.59	0.02
SR8	201.26	188.03	0.04	233.45	198.70	0.10	258.93	210.47	0.13
SR9	–	–	–	–	–	–	–	–	–
4. Deceleratory rate equations									
4.1. Phase boundary (PR) reaction									
PR1	33.34	107.18	−0.23	33.17	120.64	−0.24	39.44	127.96	−0.23
PR2	37.16	115.87	−0.24	40.37	124.56	−0.23	46.57	131.87	−0.22
PR3	38.49	117.36	−0.24	43.02	126.48	−0.23	49.19	133.81	−0.22
4.2 Based on the diffusion mechanism (DM)									
DM1	78.76	133.51	−0.17	79.22	139.19	−0.17	92.10	148.48	−0.15
DM2	12.54	105.44	−0.28	13.74	114.68	−0.28	16.67	121.05	−0.27
DM3	83.67	136.99	−0.16	88.16	143.90	−0.15	100.97	153.12	−0.14
DM4	89.06	142.85	−0.16	98.92	151.67	−0.15	111.61	160.89	−0.13
DM5	85.47	141.67	−0.17	91.72	149.49	−0.16	104.49	158.88	−0.14
DM6	100.37	146.60	−0.14	122.69	159.01	−0.10	135.12	167.65	−0.09
DM7	72.49	137.55	−0.20	70.49	143.44	−0.20	83.14	153.18	−0.18
DM8	74.53	138.18	−0.19	73.30	144.19	−0.20	86.02	153.91	−0.18
DM9	66.55	135.73	−0.21	62.40	141.32	−0.22	74.78	151.10	−0.20
DM10	13.21	106.12	−0.28	15.07	115.50	−0.28	17.98	121.90	−0.27

201.26 kJ/mol at 30°C/min, which progressively increased to 110.28, 171.87, and 233.45 kJ/mol at 40°C/min, and further to 122.85, 190.89, and 258.93 kJ/mol at 50°C/min. This trend, illustrated in Figure 8(a), indicates that higher β values require a more substantial energy input due to increased thermal degradation kinetics, which aligns with fundamental pyrolysis principles and supports these models for *Sr*WRF thermodynamic analysis.

The Gibbs free energy change (ΔG) quantifies the increase in potential energy at the saddle point of the potential energy surface, providing insights into reaction spontaneity and thermal requirements (Mian et al. 2019b). Higher ΔG values indicate less thermodynamically favorable reactions, reflecting more significant energy barriers that must be overcome. Negative ΔG values characterize exergonic (spontaneous) reactions, where the reactants have a higher free energy than the products. In contrast, positive ΔG values (observed throughout this study) signify endergonic (non-spontaneous) processes that require energy input (Raza et al. 2022b). Analysis of the best-fitted models (SR6, SR7, and SR8) revealed consistently positive ΔG values across all β values: 138.70, 163.18, and 188.03 kJ/mol at 30°C/min; 148.55, 173.42, and 198.70 kJ/mol at 40°C/min; and 157.12, 183.59, and 210.47 kJ/mol at 50°C/min. As shown in Figure 8(b), this gradual increase in ΔG with β indicates the rising energy demand for *Sr*WRF decomposition under accelerated thermal conditions.

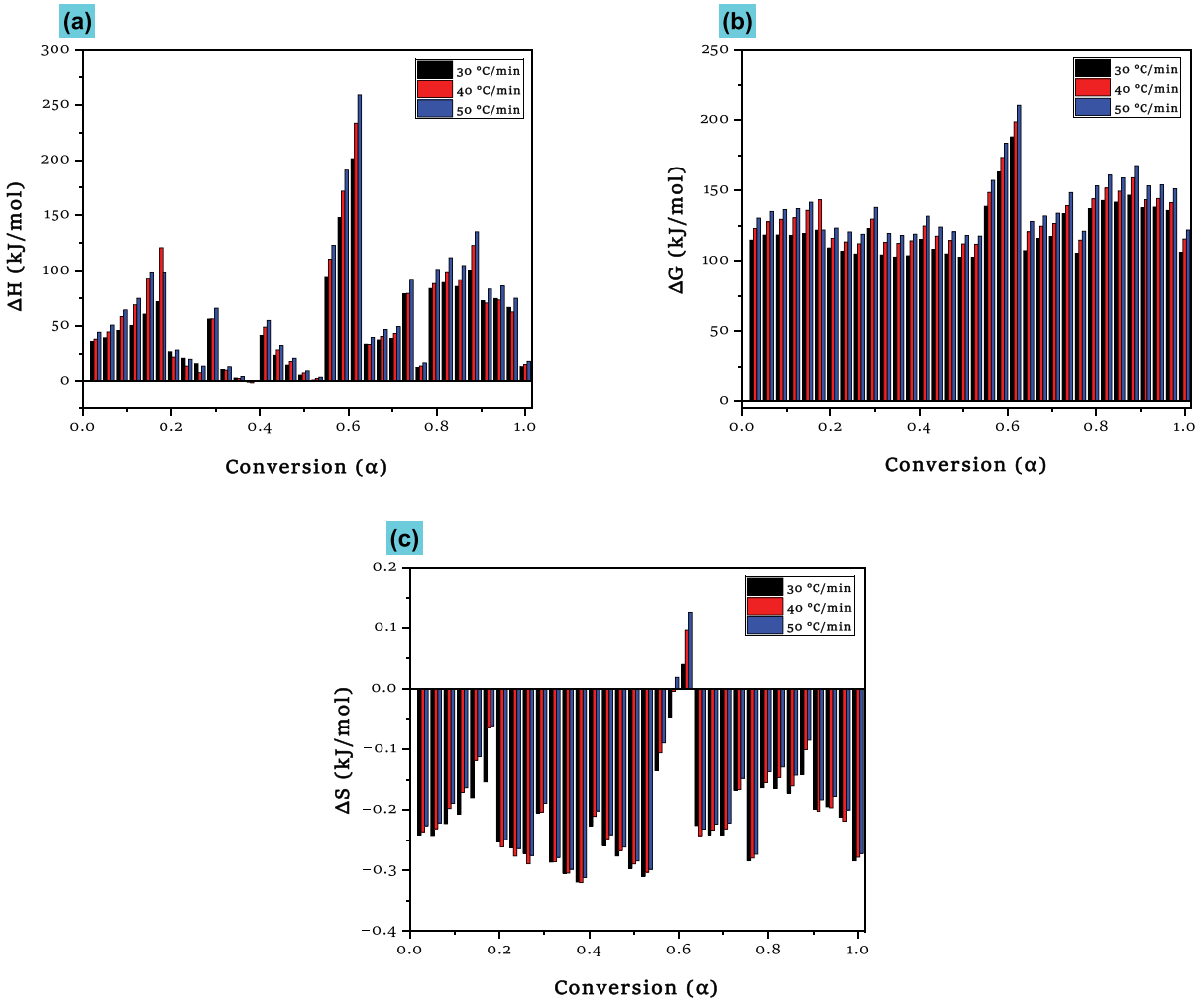

Figure 8. Variations in thermodynamic parameters ΔH, ΔS, and ΔG based on heating rate (β) and conversion rate (α).

The observed negative entropy changes (ΔS) in all models indicate that the pyrolysis products adopt more ordered molecular configurations than the original reactants, suggesting a reduction in system disorder during thermal decomposition (Naqvi, Tariq, et al. 2019). This thermodynamic behavior, also illustrated in Figure 8(c), indicates that bond dissociation in *Sr*WRFs yields degradation products with enhanced structural organization compared to the initial material. For the optimal models (SR6, SR7, and SR8), the ΔS values range from −0.09 to −0.20 kJ/mol·K, consistently showing a trend of decreasing entropy during the decomposition process. These negative ΔS values further support the conclusion that the pyrolyzed products exhibit better structural stability than the starting material.

Kinetic analysis of the active pyrolysis zone (200–650°C) was conducted using the CRM. The study revealed that increasing β from 30 to 40°C/min resulted in maximum values for E_a, Gibbs free energy change (ΔG), and enthalpy change (ΔH) across all evaluated models, further corroborated by the trends in Figure 7. These kinetic and thermodynamic parameters provide essential insights into energy demand, conversion rates, and the reaction mechanisms of the pyrolysis process. This fundamental understanding offers valuable insights for optimizing the practical applications of pyrolysis in bioenergy production (Tariq et al. 2023).

Criado master plot (CMP) method

In this study, CMP (Equation (11)) was utilized to correlate the experimental TGA data with theoretical solid-state reaction models. The models selected for analysis demonstrated high correlation coefficients (R^2

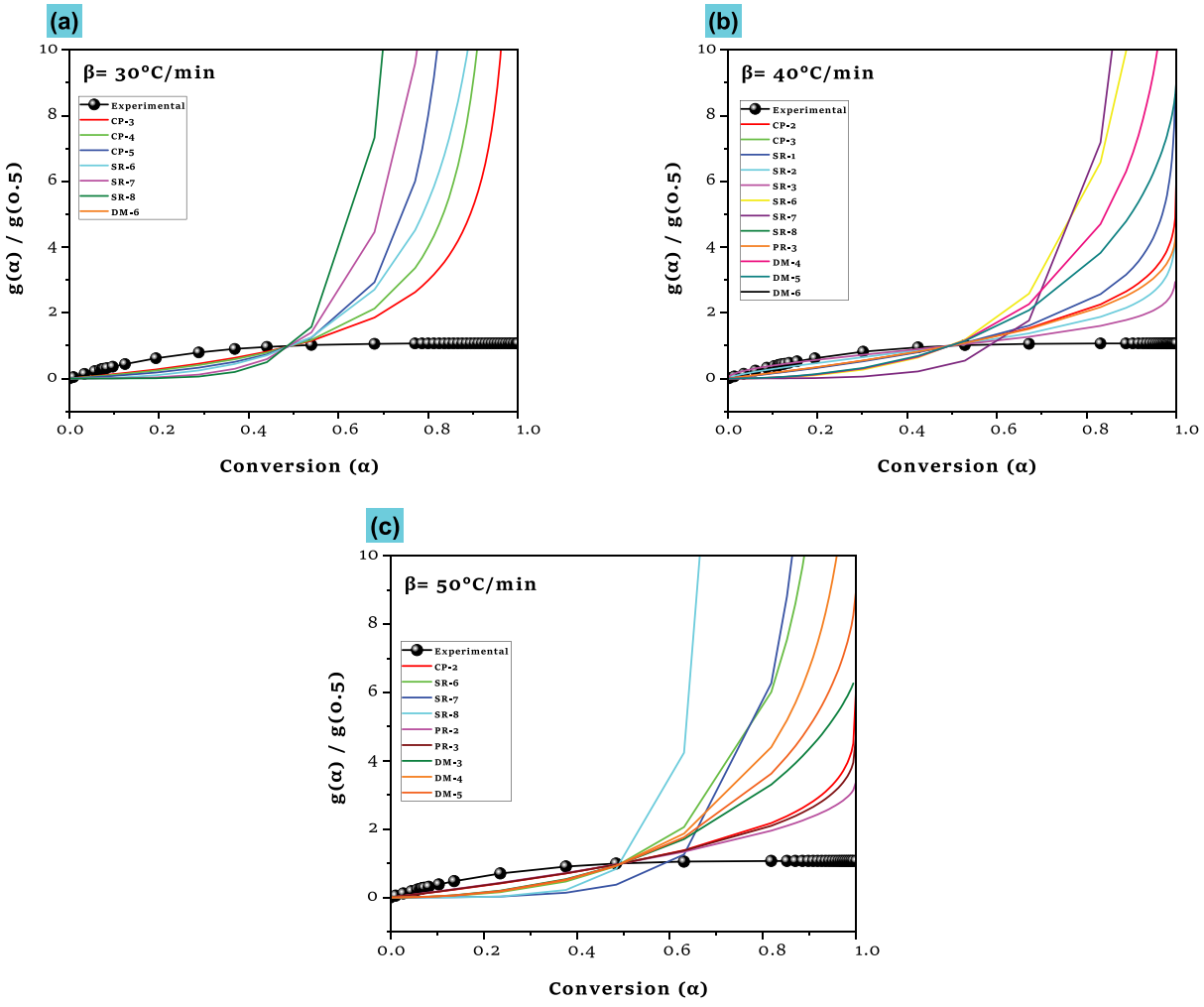

Figure 9. Criado master plot (CMP) for *Syagrus romanzoffiana* waste rachis fibers (*Sr*WRFs) at heating rates (β) of 30, 40, and 50°C/min.

≥ 0.99) across all three β values. The kinetic functions, $g(\alpha)$ and f(α), associated with each reaction mechanism are presented in Table 1.

Figure 9 displays master plots of $g(\alpha)/g(0.5)$ *vs.* α for different reaction mechanism models, produced using CMP. The experimental curve was created using WL rates obtained directly from the DTG data. The derivative weight values (%/min) from the DTG were explicitly incorporated into the experimental component of Equation (11). The most appropriate reaction model was selected by visually comparing the alignment between the experimental curve and the theoretical master plots, opting for the model that best matched the experimental data for further analysis. The alignment between the experimental data and theoretical models suggests that the pyrolysis mechanism of *Sr*WRFs may follow an SR equation or a random nucleation and growth model (SR3 model).

However, this correspondence appears most significant within a narrow conversion range, $\alpha = 0.15–0.55$, beyond which deviations occur. This observation suggests that the pyrolysis process likely involves a multi-step reaction mechanism, where no single model can fully capture the complexity of the degradation kinetics across all conversion stages. CMP offers a straightforward, model-free approach to mechanism identification by leveraging experimental DTG data. However, it has limitations; it does not account for E_a, and excluding other kinetic triplets may lower the accuracy of mechanistic conclusions.

While the Coats–Redfern method assumes a single-step reaction mechanism, it was applied here as a practical approximation to describe the main degradation stage of SrWRFs. This approach remains widely used in kinetic modeling to extract meaningful parameters, such as the activation energy (E_a) and pre-exponential factor (A), from dominant thermal events. To complement this, the master plots (CMP)

analysis was employed to capture the multi-step character of the overall pyrolysis process, particularly evident beyond a conversion degree of $\alpha = 0.55$. Together, these methods offer both simplified kinetic estimates and deeper mechanistic insights into the complex decomposition behavior of lignocellulosic biomass.

Among the tested models, the random nucleation and growth model emerged as the most plausible representation of *Sr*WRFs pyrolysis, aligning with findings from both CMP and CRM. This model emphasizes diffusion-controlled kinetics, where the release of volatiles dictates the reaction rate. The cylindrical geometry of *Sr*WRF particles further supports this mechanism, as radial diffusion through an expanding reaction zone corresponds with the assumptions of nucleation-growth theory (Khawam and Flanagan 2006).

Conclusion

The study investigates the pyrolysis behavior of *Syagrus romanzoffiana* fibers (*Sr*WRFs) through thermogravimetric analysis (TGA) under nitrogen, covering 20–800°C. Kinetic and thermodynamic analyses employed the Coats–Redfern model to determine activation energy (E_a), pre-exponential factor (A), reaction mechanisms, and thermodynamic parameters (ΔG, ΔH, ΔS) at heating rates (β) of 30, 40, and 50°C/min. Validated against literature, key findings include:

(a) Deconvolution of derivative thermogravimetry (DTG) profiles aligned with lignocellulosic decomposition mechanisms, corroborating prior biomass studies.
(b) Higher β increased E_a, reflecting thermal sensitivity and consistency with kinetic theory. SrWRFs showed optimal pyrolysis performance at 50°C/min.
(c) The SR8 model ($g(\alpha) = [-\ln(1 - \alpha)]^4$) provided the best fit, with E_a rising from 203.98 kJ/mol (30°C/min) to 262.11 kJ/mol (50°C/min).
(d) Thermodynamic analysis confirmed the process as endothermic and non-spontaneous ($\Delta H > 0$, $\Delta G > 0$), emphasizing energy-driven degradation.

These insights are critical for optimizing *Sr*WRFs in sustainable applications like biocomposites, biofuels, and bioenergy systems, where decomposition behavior dictates material design and process efficiency. The study underscores the importance of kinetic and thermodynamic parameters in advancing biomass conversion technologies.

Future studies should optimize reactors using kinetic/thermodynamic data, test *Sr*WRF-agro-residue blends for cost-efficiency, and employ machine learning for pyrolysis prediction. Catalytic pyrolysis and life-cycle analyses can boost sustainability and scalability. These advancements will integrate *Sr*WRFs into circular bioeconomy systems, enabling sustainable bioenergy production. This work establishes key groundwork for developing efficient, eco-friendly biomass conversion technologies.

Highlights

- Pyrolysis of SrWRFs was investigated at high heating rates using TGA.
- A three-Gaussian deconvolution approach separated the biomass into HCL, CL, and LG.
- Coats-Redfern kinetics identified SR8 as the best-fitting model with high E_a.
- Thermodynamics confirmed the endothermic and non-spontaneous nature of degradation.
- Kinetic compensation effect and model validation reinforced accuracy of results.

Acknowledgments

The authors are thankful to the Deanship of Graduate Studies and Scientific Research at Najran University for funding this work under the Growth Funding Program grant code (NU/GP/SERC/13/40-6).

Disclosure statement

No potential conflict of interest was reported by the author(s).

ORCID

Ahmed Belaadi http://orcid.org/0000-0002-6059-3974

Nomenclature and abbreviation

A	Pre-exponential factor (min-1)
AR	Acceleratory rate (equations)
CL	Cellulose
CMP	Criado master plot
CP	Chemical process (or mechanism that does not involve equations)
CRM	Coats-Redfern method
DM	Diffusion mechanism (deceleratory rate equations)
DTG	Derivative thermogravimetry
Ea	Activation energy (kJ/mol)
f(α)	Reaction mechanism function
g(α)	Integral expression for the reaction mechanism
h	Planck constant (6.626 x 10-34 m2.kg/s)
HCL	Hemicellulose
LG	Lignin
k(T)	Arrhenius equation
KB	Boltzmann constant (1.381 x 10-23 m2.kg/s2.K)
kiso	Isokinetic rate constant
P	Pseudo-component
PR	Phase boundary reaction (deceleratory rate equations)
R	Gas constant (0.008321 kJ/mol)
R2	Correlation coefficient
SR	Sigmoidal rate equations or random nucleation followed by growth
SrWRFs	Syagrus romanzoffiana waste rachis fibers
T	Temperature (K)
TGA	Thermogravimetric analysis
Ti	Initial decomposition temperature
Tiso	Theoretical isokinetic temperature
Tf	Final decomposition temperature
Tm	Maximum temperature at which substantial WL begins
TP	Peak temperature
WL	Weight loss
W0	Initial weight of the specimen (g)
Wf	Residual weight after the process (g)
Wi	Weight recorded at the moment of measurement (g)
α	Sample conversion
β	Heating rate (°C/min)
ΔG	Gibbs free energy
ΔS	Entropy

References

Abdel-Shafy, H. I., and M. S. M. Mansour. 2018. "Solid Waste Issue: Sources, Composition, Disposal, Recycling, and Valorization." *Egyptian Journal of Petroleum* 27 (4): 1275–1290. https://doi.org/10.1016/j.ejpe.2018.07.003.

Abubakar, I. R., K. M. Maniruzzaman, U. L. Dano, F. S. AlShihri, M. S. AlShammari, S. M. S. Ahmed, W. A. G. Al-Gehlani, and T. I. Alrawaf. 2022. "Environmental Sustainability Impacts of Solid Waste Management Practices in the Global South." *International Journal of Environmental Research and Public Health* 19 (19): 12717. https://doi.org/10.3390/ijerph191912717.

Ahmad, M. S., M. A. Mehmood, S. T. H. Taqvi, A. Elkamel, C. G. Liu, J. Xu, S. A. Rahimuddin, and M. Gull. 2017. "Pyrolysis, Kinetics Analysis, Thermodynamics Parameters and Reaction Mechanism of Typha Latifolia to Evaluate Its Bioenergy Potential." *Bioresource Technology* 245:491–501. https://doi.org/10.1016/j.biortech.2017.08.162.

Ali, I., R. Tariq, S. R. Naqvi, A. H. Khoja, M. T. Mehran, M. Naqvi, and N. Gao. 2021a. "Kinetic and Thermodynamic Analyses of Dried Oily Sludge Pyrolysis." *Journal of the Energy Institute* 95:30–40. https://doi.org/10.1016//j.joei.2020.12.002.

Ali, I., R. Tariq, S. R. Naqvi, A. H. Khoja, M. T. Mehran, M. Naqvi, and N. Gao. 2021b. "Kinetic and Thermodynamic Analyses of Dried Oily Sludge Pyrolysis." *Journal of the Energy Institute* 95:30–40. https://doi.org/10.1016/j.joei.2020.12.002.

Ali, M., A. Abdullah, N. Abdullah, A.-S. Khaled, A. Redhwan, B. Omer, S. Hilmi, A. Ahmed, and Z. Algafri. 2021. "Thermal Analyses of Loose Agave, Wheat Straw Fibers and Agave/Wheat Straw as New Hybrid Thermal Insulating Materials for Buildings." *Journal of Natural Fibers* 18 (12): 2173–2188. https://doi.org/10.1080/15440478.2020.1724232.

Amoloye, M. A., S. A. Abdulkareem, and A. G. Adeniyi. 2023. "Thermo-Kinetics, Thermodynamics, and ANN Modeling of the Pyrolytic Behaviours of Corn Cob, Husk, Leaf, and Stalk Using Thermogravimetric Analysis." *Chemical Product and Process Modeling* 18 (5): 859–876. https://doi.org/10.1515/cppm-2023-0021.

Arumugam, D. B., and M. C. Ganesan. 2024. "Catalytic Co-Pyrolysis of Bauhinia Purpurea Seed and Waste Medical Plastics for Sustainable Biofuel Production: Kinetic Analysis and Prediction Modeling." *Process Safety and Environmental Protection* 189:374–386. https://doi.org/10.1016/j.psep.2024.06.040.

Ascher, S., I. Watson, and S. You. 2022. "Machine Learning Methods for Modelling the Gasification and Pyrolysis of Biomass and Waste." *Renewable and Sustainable Energy Reviews* 155:111902. https://doi.org/10.1016/j.rser.2021.111902.

Ashraf, M., Z. Aslam, N. Ramzan, U. Aslam, A. K. Durrani, R. U. Khan, and S. Ayaz. 2023. "Pyrolysis of Cattle Dung: Model Fitting and Artificial Neural Network Validation Approach." *Biomass Conversion and Biorefinery* 13 (12): 10451–10462. https://doi.org/10.1007/s13399-021-02051-2.

Azam, M. Z., M. Ashraf, Z. Aslam, M. S. Kamal, and U. Aslam. 2024. "Combustion and Pyrolysis of Dairy Waste: A Kinetic Analysis and Prediction of Experimental Data Through Artificial Neural Network (ANN)." *Thermal Science and Engineering Progress* 53:102746. https://doi.org/10.1016/j.tsep.2024.102746.

Bongomin, O., C. Nzila, J. Igadwa Mwasiagi, and O. Maube. 2024. "Comprehensive Thermal Properties, Kinetic, and Thermodynamic Analyses of Biomass Wastes Pyrolysis via TGA and Coats-Redfern Methodologies." *Energy Conversion and Management: X* 24 (July): 100723. https://doi.org/10.1016/j.ecmx.2024.100723.

Bongomin, O., P. Nziu, and A. Akgül. 2022. "A Critical Review on the Development and Utilization of Energy Systems in Uganda." *Scientific World Journal* 2022:1–25. https://doi.org/10.1155/2022/2599467.

Chen, R., Q. Li, X. Xu, and D. Zhang. 2019. "Pyrolysis Kinetics and Reaction Mechanism of Representative Non-Charring Polymer Waste with Micron Particle Size." *Energy Conversion and Management* 198:111923. August. https://doi.org/10.1016/j.enconman.2019.111923.

Chen, R., Q. Li, Y. Zhang, X. Xu, and D. Zhang. 2019. "Pyrolysis Kinetics and Mechanism of Typical Industrial Non-Tyre Rubber Wastes by Peak-Differentiating Analysis and Multi Kinetics Methods." *Fuel* 235:1224–1237. https://doi.org/10.1016/j.fuel.2018.08.121.

Chen, W.-H., C. F. Eng, Y.-Y. Lin, and Q.-V. Bach. 2020. "Independent Parallel Pyrolysis Kinetics of Cellulose, Hemicelluloses and Lignin at Various Heating Rates Analyzed by Evolutionary Computation." *Energy Conversion and Management* 221:113165. https://doi.org/10.1016/j.enconman.2020.113165.

Choudhary, J., A. Kumar, B. Alawa, and S. Chakma. 2024. "Optimization and Prediction of Thermodynamic Parameters in Co-Pyrolysis of Banana Peel and Waste Plastics Using AIC Model and ANN Modeling." *Energy Nexus* 14 (April): 100302. https://doi.org/10.1016/j.nexus.2024.100302.

Clemente-Castro, S., A. Palma, M. Ruiz-Montoya, I. Giráldez, and M. J. Díaz. 2023. "Optimizing Pyrolysis Parameters and Product Analysis of a Fluidized Bed Pilot Plant for Leucaena Leucocephala Biomass." *Environmental Sciences Europe* 35 (1): 88. https://doi.org/10.1186/s12302-023-00800-w.

da Silva, J. C. G., J. L. F. Alves, G. D. Mumbach, S. L. F. Andersen, R. F. P. M. de Moreira, and H. J. Jose. 2022. "Torrefaction of Low-Value Agro-Industrial Wastes Using Macro-TGA with GC-TCD/FID Analysis: Physicochemical Characterization, Kinetic Investigation, and Evolution of Non-Condensable Gases." *Journal of Analytical and Applied Pyrolysis* 166 (June): 105607. https://doi.org/10.1016/j.jaap.2022.105607.

Dai, M., T. Guo, X. Hu, J. Ma, and Q. Guo. 2024. "Simulation of a 1MWth Biomass Chemical Looping Gasification Process Based on Kinetic and Pyrolysis Models." *International Journal of Hydrogen Energy* 80:298–307. https://doi.org/10.1016/j.ijhydene.2024.07.154.

Ding, Y., G. Jiang, K. Fukumoto, M. Zhao, X. Zhang, C. Wang, and C. Li. 2023. "Experimental and Numerical Simulation of Multi-Component Combustion of Typical No-Charring Material." *Energy* 262:125555. https://doi.org/10.1016/j.energy.2022.125555.

El May, Y., M. Jeguirim, S. Dorge, G. Trouvé, and R. Said. 2012. "Study on the Thermal Behavior of Different Date Palm Residues: Characterization and Devolatilization Kinetics Under Inert and Oxidative Atmospheres." *Energy* 44 (1): 702–709. https://doi.org/10.1016/j.energy.2012.05.022.

Elmay, Y., J. Mejdi, T. Gwenaelle, and R. Said. 2016. "Kinetic Analysis of Thermal Decomposition of Date Palm Residues Using Coats–Redfern Method." *Energy Sources Part A: Recovery, Utilization, and Environmental Effects* 38 (8): 1117–1124. https://doi.org/10.1080/15567036.2013.821547.

Ferfari, O., A. Belaadi, A. Bedjaoui, H. Alshahrani, and M. K. A. Khan. 2023. "Characterization of a New Cellulose Fiber Extracted from Syagrus romanzoffiana Rachis as a Potential Reinforcement in Biocomposites Materials." *Materials Today Communications* 36 (May): 106576. https://doi.org/10.1016/j.mtcomm.2023.106576.

Ferfari, O., A. Belaadi, M. Bourchak, D. Ghernaout, R. M. Ajaj, and B. X. Chai. 2024. "Thermal Decomposition of Syagrus Romanzoffiana Palm Fibers: Thermodynamic and Kinetic Studies Using the Coats-Redfern Method." *Renewable Energy* 231 (July): 120928. https://doi.org/10.1016/j.renene.2024.120928.

Fernandez, A., S. A, M. Gr, and R. Rodriguez. 2017. "Nonisothermal Drying Kinetics of Biomass Fuels by Thermogravimetric Analysis Under Oxidative and Inert Atmosphere." *Drying Technology* 35 (2): 163–172. https://doi.org/10.1080/07373937.2016.1163265.

Fernandez, A., P. Sette, M. Echegaray, J. Soria, D. Salvatori, G. Mazza, and R. Rodriguez. 2023a. "Clean Recovery of Phenolic Compounds, Pyro-Gasification Thermokinetics, and Bioenergy Potential of Spent Agro-Industrial Bio-Wastes." *Biomass Conversion and Biorefinery* 13 (14): 12509–12526. https://doi.org/10.1007///s13399-021-02197-z.

Fernandez, A., P. Sette, M. Echegaray, J. Soria, D. Salvatori, G. Mazza, and R. Rodriguez. 2023b. "Clean Recovery of Phenolic Compounds, Pyro-Gasification Thermokinetics, and Bioenergy Potential of Spent Agro-Industrial Bio-Wastes." *Biomass Conversion and Biorefinery* 13 (14): 12509–12526. https://doi.org/10.1007//s13399-021/-02197-z.

Ferronato, N., and V. Torretta. 2019. "Waste Mismanagement in Developing Countries: A Review of Global Issues." *International Journal of Environmental Research and Public Health* 16 (6): 1060. https://doi.org/10.3390/ijerph16061060.

Fischer, O., R. Lemaire, and A. Bensakhria. 2024. "Thermogravimetric Analysis and Kinetic Modeling of the Pyrolysis of Different Biomass Types by Means of Model-Fitting, Model-Free and Network Modeling Approaches." *Journal of Thermal Analysis and Calorimetry* 149 (19): 10941–10963. https://doi.org/10.1007/s10973-023-12868-w.

Gayathri, K., K. Rajesh, P. Krishnan, K. Anandan, R. Swadhi, A. R. Devaraj, and G. Anbalagan. 2020. "A Study on Kinetic Properties of Brucinium Hydrogen (S) Malate Pentahydrate Single Crystal by Coats Redfern Method." *AIP Conference Proceedings* 2265 (1): 30425. https://doi.org/10.1063/5.0017481.

Gupta, R., Z. H. Ouderji, Y. Uzma, Z. W. T. Sloan, and S. You. 2024. "Machine Learning for Sustainable Organic Waste Treatment: A Critical Review." *NPJ Materials Sustainability* 2 (1): 5. https://doi.org/10.1038/s44296-024-00009-9.

Hadou, A., A. Belaadi, I. M. H. Alshaikh, and D. Ghernaout. 2024a. "Pyrolysis Features of Dracaena Draco Lignocellulosic Fibers: Kinetic and Thermodynamic Analysis at Various Heating Rates Through Coats-Redfern Method." *Case Studies in Thermal Engineering* 64 (October): 105406. https://doi.org/10.1016//j.csite/.2024.105406.

Hadou, A., A. Belaadi, I. M. H. Alshaikh, and D. Ghernaout. 2024b. "Pyrolysis Features of Dracaena Draco Lignocellulosic Fibers: Kinetic and Thermodynamic Analysis at Various Heating Rates Through Coats-Redfern Method." *Case Studies in Thermal Engineering* 64 (November): 105406. https://doi.org/10.1016//j.csite.2024/.105406.

Hadou, A., A. Belaadi, D. Ghernaout, and H. Mukalazi. 2025. "Forecasting the Thermal Degradation Depending on the Kinetics of Dracaena Draco Lignocellulosic Fibers Using an Artificial Neural Network." *Journal of Natural Fibers* 22 (1): 1–26. https://doi.org/10.1080/15440478.2025.2531368.

Hidayat, S., M. S. A. Bakar, A. Ahmed, D. A. Iryani, M. Hussain, F. Jamil, and Y.-K. Park. 2021. "Comprehensive Kinetic Study of Imperata Cylindrica Pyrolysis via Asym2sig Deconvolution and Combined Kinetics." *Journal of Analytical and Applied Pyrolysis* 156:105133. https://doi.org/10.1016/j.jaap.2021//.105133.

Hidayat, S., M. S. A. Bakar, A. Ahmed, D. A. Iryani, M. Hussain, F. Jamil, and Y. K. Park. 2021. "Comprehensive Kinetic Study of Imperata Cylindrica Pyrolysis via Asym2sig Deconvolution and Combined Kinetics." *Journal of Analytical and Applied Pyrolysis* 156 (April): 105133. https://doi.org/10.1016/j.jaap.2021///.105133.

Huang, L., J. Liu, Y. He, S. Sun, J. Chen, J. Sun, K. Chang, J. Kuo, and X. Ning. 2016. "Thermodynamics and Kinetics Parameters of Co-Combustion Between Sewage Sludge and Water Hyacinth in CO2/O2 Atmosphere as Biomass to Solid Biofuel." *Bioresource Technology* 218:631–642. https://doi.org/10.1016/j.biortech.2016.06.133.

Huang, Z., F. He, H. Zhu, D. Chen, K. Zhao, G. Wei, Y. Feng, A. Zheng, Z. Zhao, and H. Li. 2015a. "Thermodynamic Analysis and Thermogravimetric Investigation on Chemical Looping Gasification of Biomass Char Under Different Atmospheres with Fe2O3 Oxygen Carrier." *Applied Energy* 157:546–553. https://doi.org/10.1016//j.apenergy.2015.03.033.

Huang, Z., F. He, H. Zhu, D. Chen, K. Zhao, G. Wei, Y. Feng, A. Zheng, Z. Zhao, and H. Li. 2015b. "Thermodynamic Analysis and Thermogravimetric Investigation on Chemical Looping Gasification of Biomass Char Under Different Atmospheres with Fe2O3 Oxygen Carrier." *Applied Energy* 157:546–553. https://doi.org/10.1016/j.apenergy/.2015.03.033.

Jiang, L., D. Zhang, M. Li, J.-J. He, Z.-H. Gao, Y. Zhou, and J.-H. Sun. 2018. "Pyrolytic Behavior of Waste Extruded Polystyrene and Rigid Polyurethane by Multi Kinetics Methods and Py-GC/MS." *Fuel* 222:11–20. https://doi.org/10.1016/j.fuel.2018.02.143.

Khawam, A., and D. R. Flanagan. 2006. "Solid-State Kinetic Models: Basics and Mathematical Fundamentals." *The Journal of Physical Chemistry B* 110 (35): 17315–17328. https://doi.org/10.1021/jp062746a.

Kumar, M., P. K. Mishra, and S. N. Upadhyay. 2020. "Thermal Degradation of Rice Husk: Effect of Pre-Treatment on Kinetic and Thermodynamic Parameters." *Fuel* 268:117164. https://doi.org/10.1016/j.fuel.2020.117164.

Kumar, M., D. Rai, G. Bhardwaj, S. N. Upadhyay, and P. K. Mishra. 2021. "Pyrolysis of Peanut Shell: Kinetic Analysis and Optimization of Thermal Degradation Process." *Industrial Crops and Products* 174 (October): 114128. https://doi.org/10.1016/j.indcrop.2021.114128.

Kumar Shrivastava, D., and J. Prasad Chakraborty. 2024. "Estimation of Kinetic and Thermodynamic Parameters During Thermal Decomposition of Raw, Boiled, and Torrefied Banana Peel Through Arrhenius and CR Methods." *Thermal Science and Engineering Progress* 53:102696. https://doi.org/10.1016/j.tsep.2024.102696.

Kumar, V. K., S. C. Hallad, and N. L. Panwar. 2024. "Thermogravimetric Pyrolysis Investigation of Pistachio Shell for Its Potential of Thermal Properties, Kinetics and Thermodynamics." *Discover Energy* 4 (1). https://doi.org/10.1007/s43937-024-00030-y.

Lalaymia, I., A. Bedjaoui, A. Belaadi, M. M. S. Abdullah, D. Ghernaout, and A. Al-Khawlani. 2024. "Slow Pyrolysis of Agave Americana L. Fibers: Analysis of Kinetics and Thermodynamics Using the Coats-Redfern Method at Different Heating Rates." *Industrial Crops and Products* 219 (March): 119043. https://doi.org/10.1016/j.indcrop.2024.119043 .

Lalaymia, I., A. Belaadi, H. Alshahrani, D. Ghernaout, and H. Mukalazi. 2025. "Sustainable Renewable Biofuel Production Toward Pyrolysis of Fibers Biowaste Agave americana L. and Thermodynamics Mechanisms Kinetic Parameters Triplet Assessment." *Journal of Natural Fibers* 22 (1): 1–25. https://doi.org/10.1080/15440478.2025.2537069.

Lei, J., X. Ye, H. Wang, and D. Zhao. 2023. "Insights into Pyrolysis Kinetics, Thermodynamics, and the Reaction Mechanism of Wheat Straw for Its Resource Utilization." *Sustainability (Switzerland)* 15 (16): 12536. https://doi.org/10.3390/su151612536.

Li, B., J.-H. Ng, K. S. Woon, W. W. F. Chong, K. L. A. Ng, C. T. Lee, M. C. Chiong, K. S. Nge, and G. R. Mong. 2024. "Comparative Analysis of Kinetic Model-Fitting Methods and Selection Priority for Horse Manure Pyrolysis." *Sustainable Chemistry and Pharmacy* 39:101590. https://doi.org/10.1016/j.scp.2024.101590.

Li, B. Y., M. Y. Tee, K. S. Nge, A. K. L. Ng, W. W. F. Chong, J. H. Ng, and G. R. Mong. 2023. "Comparison Kinetic Analysis Between Coats-Redfern and Criado's Master Plot on Pyrolysis of Horse Manure." *Chemical Engineering Transactions* 106 (June): 1273–1278. https://doi.org/10.3303/CET23106213.

Lingamdinne, L. P., G. K. R. Angaru, C. A. Pal, J. R. Koduru, R. R. Karri, N. M. Mubarak, and Y.-Y. Chang. 2024. "Insights into Kinetics, Thermodynamics, and Mechanisms of Chemically Activated Sunflower Stem Biochar for Removal of Phenol and Bisphenol-A from Wastewater." *Scientific Reports* 14 (1): 4267. https://doi.org/10.1038/s41598-024-54907-y.

Liu, J., H. Lyu, C. Cheng, Z. Xu, and W. Zhang. 2024. "Enhancing Pyrolysis Process Monitoring and Prediction for Biomass: A Machine Learning Approach." *Fuel* 362:130873. https://doi.org/10.1016/j.fuel.2024.130873.

Ma, C., F. Zhang, J. Hu, H. Wang, S. Yang, and H. Liu. 2023. "Co-Pyrolysis of Sewage Sludge and Waste Tobacco Stem: Gas Products Analysis, Pyrolysis Kinetics, Artificial Neural Network Modeling, and Synergistic Effects." *Bioresource Technology* 389:129816. https://doi.org/10.1016/j.biortech.2023.129816.

Mian, I., X. Li, Y. Jian, O. D. Dacres, M. Zhong, J. Liu, F. Ma, and N. Rahman. 2019a. "Kinetic Study of Biomass Pellet Pyrolysis by Using Distributed Activation Energy Model and Coats Redfern Methods and Their Comparison." *Bioresource Technology* 294:122099. https://doi.org/10.1016/j.biortech/.2019.122099.

Mian, I., X. Li, Y. Jian, O. D. Dacres, M. Zhong, J. Liu, F. Ma, and N. Rahman. 2019b. "Kinetic Study of Biomass Pellet Pyrolysis by Using Distributed Activation Energy Model and Coats Redfern Methods and Their Comparison." *Bioresource Technology* 294 (September): 122099. https://doi.org/10.1016//j.biortech.2019.122099.

Mishra, A., S. Nanda, M. Ranjan Parida, P. K. Jena, S. K. Dwibedi, S. Manjari Samantaray, D. Samantaray, M. K. Mohanty, and M. Dash. 2023. "A Comparative Study on Pyrolysis Kinetics and Thermodynamic Parameters of Little Millet and Sunflower Stems Biomass Using Thermogravimetric Analysis." *Bioresource Technology* 367:128231. November. https://doi.org/10.1016/j.biortech.2022.128231.

Najafi, H., Z. Rezaei Laye, and M. A. Sobati. 2024. "Thermal Conversion Potential of Tea Stems: Experimental Investigation, Reaction Mechanism, and Kinetic Modeling." *Industrial Crops and Products* 207:117753. https://doi.org/10.1016/j.indcrop.2023.117753.

Naqvi, S. R., I. Ali, S. Nasir, S. Ali Ammar Taqvi, A. E. Atabani, and W.-H. Chen. 2020. "Assessment of Agro-Industrial Residues for Bioenergy Potential by Investigating Thermo-Kinetic Behavior in a Slow Pyrolysis Process." *Fuel* 278:118259. https://doi.org/10.1016/j.fuel.2020.118259.

Naqvi, S. R., Z. Hameed, R. Tariq, S. A. Taqvi, I. Ali, M. B. K. Niazi, T. Noor, A. Hussain, N. Iqbal, and M. Shahbaz. 2019. "Synergistic Effect on Co-Pyrolysis of Rice Husk and Sewage Sludge by Thermal Behavior, Kinetics, Thermodynamic Parameters and Artificial Neural Network." *Waste Management* 85:131–140. https://doi.org/10.1016/j.wasman.2018.12.031.

Naqvi, S. R., R. Tariq, Z. Hameed, I. Ali, M. Naqvi, W.-H. Chen, S. Ceylan, et al. 2019. "Pyrolysis of High Ash Sewage Sludge: Kinetics and Thermodynamic Analysis Using Coats-Redfern Method." *Renewable Energy* 131:854–860. https://doi.org/10.1016/j.renene.2018.07.094.

Naqvi, S. R., Y. Uemura, N. Osman, and S. Yusup. 2015. "Kinetic Study of the Catalytic Pyrolysis of Paddy Husk by Use of Thermogravimetric Data and the Coats–Redfern Model." *Research on Chemical Intermediates* 41 (12): 9743–9755. https://doi.org/10.1007/s11164-015-1962-0.

Nasfi, M., M. Carrier, and S. Salvador. 2022. "Reconsidering the Potential of Micropyrolyzer to Investigate Biomass Fast Pyrolysis Without Heat Transfer Limitations." *Journal of Analytical and Applied Pyrolysis* 165:105582. https://doi.org/10.1016/j.jaap.2022.105582.

Nath, S. 2024. "Biotechnology and Biofuels: Paving the Way Towards a Sustainable and Equitable Energy for the Future." *Discover Energy* 4 (1). https://doi.org/10.1007/s43937-024-00032-w.

Osman, A. I., B. Fang, Y. Zhang, Y. Liu, J. Yu, M. Farghali, A. K. Rashwan, et al. 2024. "Life Cycle Assessment and Techno-Economic Analysis of Sustainable Bioenergy Production: A Review." *Environmental Chemistry Letters* 22 (3). Springer International Publishing. 1115–1154. https://doi.org/10.1007/s10311-023-01694-z.

Osman, A. I., M. Nasr, M. Farghali, A. K. Rashwan, A. Abdelkader, A. H. Al-Muhtaseb, I. Ihara, and D. W. Rooney. 2024. "Optimizing Biodiesel Production from Waste with Computational Chemistry, Machine Learning and Policy Insights: A Review." *Environmental Chemistry Letters* 22 (3). Springer International Publishing. 1005–1071. https://doi.org/10.1007/s10311-024-01700-y.

Ozyuguran, A., A. Akturk, and S. Yaman. 2018. "Optimal Use of Condensed Parameters of Ultimate Analysis to Predict the Calorific Value of Biomass." *Fuel* 214:640–646. October. https://doi.org/10.1016/j.fuel.2017.10.082.

Pal, D. B., N. Srivastava, S. L. Pal, M. Kumar, A. Syed, A. M. Elgorban, R. Singh, and V. K. Gupta. 2021. "Lignocellulosic Composition Based Thermal Kinetic Study of Mangiferaindica Lam, Artocarpus Heterophyllus Lam and Syzygium Jambolana Seeds." *Bioresource Technology* 341:125891. September. https://doi.org/10.1016/j.biortech.2021.125891.

Poletto, M., H. L. Ornaghi Jnior, and A. J. Zattera. 2015. "Thermal Decomposition of Natural Fibers: Kinetics and Degradation Mechanisms." *Reactions and Mechanisms in Thermal Analysis of Advanced Materials* (July). https://doi.org/10.1002/9781119117711.ch21.

Rasam, S., A. Moshfegh Haghighi, K. Azizi, A. Soria-Verdugo, and M. Keshavarz Moraveji. 2020. "Thermal Behavior, Thermodynamics and Kinetics of Co-Pyrolysis of Binary and Ternary Mixtures of Biomass through Thermogravimetric Analysis." *Fuel* 280:118665. https://doi.org/10.1016/j.fuel.2020.118665.

Rashd, J. A., J. Lalung, M. A. Kassim, D. Wijaya, A. M. M. Allzrag, and M. A. Shaah. 2024. "Kinetics and Thermodynamic Studies on Biodiesel Synthesis via Soxhlet Extraction of Scenedesmus parvus Algae Oil." *Energy Conversion and Management: X* 23 (March): 100633. https://doi.org/10.1016/j.ecmx.2024.100633.

Raza, M., and B. Abu-Jdayil. 2023. "Synergic Interactions, Kinetic and Thermodynamic Analyses of Date Palm Seeds and Cashew Shell Waste Co-Pyrolysis Using Coats–Redfern Method." *Case Studies in Thermal Engineering* 47 (May): 103118. https://doi.org/10.1016/j.csite.2023.103118.

Raza, M., B. Abu-Jdayil, A. H. Al-Marzouqi, and A. Inayat. 2022a. "Kinetic and Thermodynamic Analyses of Date Palm Surface Fibers Pyrolysis Using Coats-Redfern Method." *Renewable Energy* 183:67–77. https://doi.org/10.1016/j.renene/.2021.10.065.

Raza, M., B. Abu-Jdayil, A. H. Al-Marzouqi, and A. Inayat. 2022b. "Kinetic and Thermodynamic Analyses of Date Palm Surface Fibers Pyrolysis Using Coats-Redfern Method." *Renewable Energy* 183:67–77. https://doi.org/10.1016/j.renene/.2021/.10.065.

Raza, M., B. Abu-Jdayil, and A. Inayat. 2023. "Pyrolytic Kinetics and Thermodynamic Analyses of Date Seeds at Different Heating Rates Using the Coats–Redfern Method." *Fuel* 342:127799. https://doi.org/10.1016/j.fuel.2023.127799.

Reddy, K. V., N. R. Satya Sree, P. Ranjit, and N. R. Maddela. 2023. *Chapter 23 - Biomass Waste and Feedstock as a Source of Renewable Energy* (M. P. B. T.-G. A. to A. F. for a S. F. Shah (Edited by); pp. 325–334). Elsevier. https://doi.org/10.1016/B978-0-12-824318-3.00033-3.

Sait, H. H., A. Hussain, A. A. Salema, and F. N. Ani. 2012. "Pyrolysis and Combustion Kinetics of Date Palm Biomass Using Thermogravimetric Analysis." *Bioresource Technology* 118:382–389. https://doi.org/10.1016/j.biortech.2012.04.081.

Samuel Olugbenga, O., P. Goodness Adeleye, S. Blessing Oladipupo, A. Timothy Adeleye, and K. Igenepo John. 2024. "Biomass-Derived Biochar in Wastewater Treatment- A Circular Economy Approach." *Waste Management Bulletin* 1 (4): 1–14. https://doi.org/10.1016/j.wmb.2023.07.007.

Silvestre, W. P., G. F. Pauletti, and C. Baldasso. 2020. "Fodder Radish (Raphanus Sativus L.) Seed Cake as a Feedstock for Pyrolysis." *Industrial Crops and Products* 154 (June): 112689. https://doi.org/10.1016/j.indcrop.2020.112689.

Sobek, S., and S. Werle. 2020. "Kinetic Modelling of Waste Wood Devolatilization During Pyrolysis Based on Thermogravimetric Data and Solar Pyrolysis Reactor Performance." *Fuel* 261:116459. October. https://doi.org/10.1016/j.fuel.2019.116459.

Steven, S., P. Hernowo, N. Nadirah, I. Febijanto, R. Herdioso, D. Dharmawan, E. S. A. Soekotjo, and Y. Bindar. 2024. "Transformation Method in Determining Kinetic Parameters of Biomass Thermal Decomposition from Solid-State Approach to Volatile State Approach." *Biomass & Bioenergy* 183:107171. https://doi.org/10.1016/j.biombioe.2024.107171.

Sun, K., M. Cui, B. Zhang, Y. Li, P. Geng, P. Fu, W. Yi, and Y. Zhang. 2023. "Some New Insights into the Kinetic Compensation Effect in Different Diffusion-Controlled Domain for Char-CO2 Gasification." *Renewable Energy* 217:119355. https://doi.org/10.1016/j.renene.2023.119355.

Sun, S., Y. Yuan, R. Chen, X. Xu, and D. Zhang. 2021. "Kinetic, Thermodynamic and Chemical Reaction Analyses of Typical Surgical Face Mask Waste Pyrolysis." *Thermal Science and Engineering Progress* 26 (July): 101135. https://doi.org/10.1016/j.tsep.2021.101135.

Tabal, A., A. Barakat, A. Aboulkas, and K. El Harfi. 2021. "Pyrolysis of Ficus Nitida Wood: Determination of Kinetic and Thermodynamic Parameters." *Fuel* 283:119253. https://doi.org/10.1016/j.fuel.2020.119253.

Tariq, R., A. Inayat, M. Shahbaz, H. Zeb, C. Ghenai, T. Al-Ansari, and J. Kim. 2023. "Kinetic and Thermodynamic Evaluation of Pyrolysis of Jeans Waste via Coats-Redfern Method." *The Korean Journal of Chemical Engineering* 40 (1): 155–161. https://doi.org/10.1007/s11814-022-1248-3.

Torres-Sciancalepore, R., M. Riveros-Gomez, D. Zalazar-García, D. Asensio, M. P. Fabani, R. Rodriguez, G. Fouga, and G. Mazza. 2023. "Two-Step Valorization of Invasive Species Rosa Rubiginosa L. Husk Waste Through Eco-Friendly

Optimized Pectin Extraction and Subsequent Pyrolysis." *Journal of Environmental Chemical Engineering* 11 (5). Elsevier. 110802. https://doi.org/10.1016/j.jece.2023.110802.
Umezawa, T. 2018. "Lignin Modification in Planta for Valorization." *Phytochemistry Reviews* 17 (6): 1305–1327. https://doi.org/10.1007/s11101-017-9545-x.
Vanisree, G. S., A. M. Chandran, and K. Aparna. 2024. "Investigation on Thermochemical Characteristics and Pyrolysis Kinetics of Lignocellulosic Biomass for Biofuel Production Feasibility." *Biomass Conversion and Biorefinery*. https://doi.org/10.1007/s13399-024-05657-4.
Vyazovkin, S., A. K. Burnham, J. M. Criado, L. A. Pérez-Maqueda, C. Popescu, and N. Sbirrazzuoli. 2011. "ICTAC Kinetics Committee Recommendations for Performing Kinetic Computations on Thermal Analysis Data." *Thermochimica Acta* 520 (1): 1–19. https://doi.org/10.1016/j.tca.2011.03.034.
Vyazovkin, S., and N. Muravyev. 2024. "Single Heating Rate Methods Are a Faulty Approach to Pyrolysis Kinetics." *Biomass Conversion and Biorefinery* 14 (15): 16879–16881. https://doi.org/10.1007/s13399-022-03735-z.
Wang, J., D. Yellezuome, Z. Zhang, S. Liu, J. Lu, P. Zhang, S. Zhang, et al. 2022. "Understanding Pyrolysis Mechanisms of Pinewood Sawdust and Sugarcane Bagasse from Kinetics and Thermodynamics." *Industrial Crops and Products* 177 (August 2021): 114378. https://doi.org/10.1016/j.indcrop.2021.114378.
Wang, L., R. Zhang, J. Li, L. Guo, H. Yang, F. Ma, and H. Yu. 2018. "Comparative Study of the Fast Pyrolysis Behavior of Ginkgo, Poplar, and Wheat Straw Lignin at Different Temperatures." *Industrial Crops and Products* 122 (June): 465–472. https://doi.org/10.1016/j.indcrop.2018.06.038.
Wang, Y., S. Yang, G. Bao, and H. Wang. 2023a. "Investigation of Tobacco Straw Pyrolysis: Three-Parallel Gaussian Reaction Modeling, Products Analysis and ANN Application." *Industrial Crops and Products* 200 (PB): 116864. https://doi.org/10.1016/j.indcrop/.2023/.116864.
Wang, Y., S. Yang, G. Bao, and H. Wang. 2023b. "Investigation of Tobacco Straw Pyrolysis: Three-Parallel Gaussian Reaction Modeling, Products Analysis and ANN Application." *Industrial Crops and Products* 200:116864. https://doi.org/10.1016/j.indcrop.2023/.116864.
Wang, Y., S. Yang, G. Bao, and H. Wang. 2024a. "Investigation on Prospective Bioenergy from Pyrolysis of Macadamia Nut Shell Waste Using Multicomponent Fraser-Suzuki Kinetic Model, Kinetic Triplet and Thermodynamic Parameters." *Journal of the Energy Institute* 114:101611. https://doi.org/10.1016/j.joei.2024.101611.
Wang, Y., S. Yang, G. Bao, and H. Wang. 2024b. "Pyrolysis of Macadamia Nut Peel Using Multicomponent Gaussian Kinetic Modeling and ANN Analysis." *Biomass & Bioenergy* 183:107170. December. https://doi.org/10.1016/j.biombioe.2024/.107170.
Wang, Y., S. Yang, G. Bao, and H. Wang. 2024c. "Pyrolysis of Macadamia Nut Peel Using Multicomponent Gaussian Kinetic Modeling and ANN Analysis." *Biomass & Bioenergy* 183:107170. https://doi.org/10.1016/j.biombioe//.2024.107170.
Wu, Y., J. Du, G. Liu, D. Ma, F. Jia, J. J. Klemeš, and J. Wang. 2022. "A Review of Self-Cleaning Technology to Reduce Dust and Ice Accumulation in Photovoltaic Power Generation Using Superhydrophobic Coating." *Renewable Energy* 185:1034–1061. https://doi.org/10.1016/j.renene.2021.12.123.
Yao, F., Q. Wu, Y. Lei, W. Guo, and Y. Xu. 2008. "Thermal Decomposition Kinetics of Natural Fibers: Activation Energy with Dynamic Thermogravimetric Analysis." *Polymer Degradation & Stability* 93 (1): 90–98. https://doi.org/10.1016/j.polymdegradstab.2007.10.012.
Zhang, P., T. Zhang, J. Zhang, H. Liu, C. Chicaiza-Ortiz, J. T. E. Lee, Y. He, Y. Dai, and Y. W. Tong. 2024. "A Machine Learning Assisted Prediction of Potential Biochar and Its Applications in Anaerobic Digestion for Valuable Chemicals and Energy Recovery from Organic Waste." *Carbon Neutrality* 3 (1). https://doi.org/10.1007/s43979-023-00078-0.
Zhao, C., E. Jiang, and A. Chen. 2017. "Volatile Production from Pyrolysis of Cellulose, Hemicellulose and Lignin." *Journal of the Energy Institute* 90 (6): 902–913. https://doi.org/10.1016/j.joei.2016.08.004.
Zhong, Y., Y. Ding, G. Jiang, K. Lu, and C. Li. 2023. "Comparison of Artificial Neural Networks and Kinetic Inverse Modeling to Predict Biomass Pyrolysis Behavior." *Journal of Analytical and Applied Pyrolysis* 169:105802. https://doi.org/10.1016/j.jaap.2022.105802.
Zhu, H., Z. Dong, X. Yu, G. Cunningham, J. Umashanker, X. Zhang, A. V. Bridgwater, and J. Cai. 2021. "A Predictive PBM-DEAM Model for Lignocellulosic Biomass Pyrolysis." *Journal of Analytical and Applied Pyrolysis* 157:105231. https://doi.org/10.1016/j.jaap.2021.105231.
Zikhali, V. N., C. Mpofu, D. Nyama, B. Nyoni, and K. Mushonga. 2023. "Kinetic and Thermodynamic Analysis of Chicken Manure Pyrolysis for Sustainable Waste Management in the Poultry Industry." *Scholars International Journal of Chemistry and Material Sciences* 6 (6): 135–140. https://doi.org/10.36348/sijcms.2023.v06i06.003.
Zong, P., Y. Jiang, Y. Tian, J. Li, M. Yuan, Y. Ji, M. Chen, D. Li, and Y. Qiao. 2020. "Pyrolysis Behavior and Product Distributions of Biomass Six Group Components: Starch, Cellulose, Hemicellulose, Lignin, Protein and Oil." *Energy Conversion and Management* 216:112777. https://doi.org/10.1016/j.enconman.2020.112777.